339

The Surface Downward Longwave Radiation in the ECMWF Forecast system

Jean-Jacques Morcrette

Research Department

July 2001

For additional copies please contact

The Library
ECMWF
Shinfield Park
Reading, Berks RG2 9AX

library@ecmwf.int

Series: ECMWF Technical Memoranda

A full list of ECMWF Publications can be found on our web site under:
http://www.ecmwf.int/pressroom/publications.html

ABSTRACT

The surface downward longwave radiation, computed by the ECMWF forecast system used for the 40-year reanalysis, is compared with surface radiation measurements for the April-May 1999 period, available as part of the BSRN, SURFRAD and ARM programs. Emphasis is put on comparisons on a one-hour basis, as this allows discrepancies to be more easily linked to differences between model description and observations of temperature, humidity and cloud. It also allows to compare the model and observed temporal variability in the surface radiation fluxes.

Comparisons are first carried out at locations for which the spectral model orography differs from the actual station height. Sensitivity of the model fluxes to various algorithms to correct for this discrepancy is explored. A simple interpolation/extrapolation scheme for pressure, temperature and humidity allows to improve the longwave and shortwave surface fluxes in most cases.

Intercomparisons of surface longwave radiation are presented for the various longwave radiation schemes operational since the 15-year ECMWF reanalysis (ERA-15) was performed. The Rapid Radiation Transfer Model of Mlawer et al. (1997), now operational at ECMWF, is shown to correct for the major underestimation in clear-sky downward longwave radiation seen in ERA-15.

Sensitivity calculations are also carried out to explore the role of the cloud optical properties, cloud effective particle size, and aerosols in the representation of the surface downward longwave radiation.

1. Introduction

With the efforts at NCEP (National Center for Environmental Prediction), NASA DAO (National Aeronautics and Space Administration, Data Assimilation Office) and ECMWF (European Centre for Medium-Range Weather Forecasts) to re-analyse, first fifteen (1979-1993), then forty (1958-1997) years of meteorological data, consistent long time series of atmospheric fields of temperature, humidity and winds are becoming available. As by-products of these re-analyses, a large number of the quantities produced by the parametrizations of the physical processes is archived, which can then be compared to observations not assimilated in the analysis process. Among other radiative fluxes and heating rates, one such parameter is the longwave (LW) radiation at the surface, which mainly depends on the temperature and water vapour distribution in the planetary boundary layer and on the presence of clouds in the first few kilometres above the surface. Various authors have aimed at deriving this surface longwave flux from satellite observations, particularly from ISCCP, (Darnell et al., 1983, 1992; Gupta et al., 1993, 1999; Rossow and Zhang, 1995), which would help in the validation of the radiation fields produced by general circulation climate models (GCMs). In this case, such a validation is usually done on the monthly time-scale provided by these climatological datasets. Another possibility of validation of the surface longwave radiation produced by GCMs has emerged from the advent of a variety of surface networks carrying out well calibrated surface radiation measurements. All of this recent validation effort has indicated a general underestimation of the downward longwave radiation at the surface in climate GCMs and in ERA-15 (Garratt et al., 1993; Garratt and Prata, 1996, Garratt et al., 1998; Wild et al., 1995, 2001).

Most of these GCM studies have focussed on comparisons performed on monthly mean time-scales, and of point measurements with model radiation fluxes representative of grids, the size of which is usually of the order of 10^4 to 10^5 km^2. Moreover, in the case of the climate GCMs, the verification is further complicated by the model integration having possibly drifted away from the observed profiles in terms of temperature, humidity and clouds. Wild et al. (2001) questioned the adequacy of the present generation of GCM-type LW radiation schemes at representing the clear-sky downward LW radiation. Apart from deficiencies in the absorption parameters used in the radiation schemes, Wild (1999) also explored the role of aerosols produced by biomass burning, particularly for surface downward shortwave radiation. One might also wonder whether some of the biases found in the previously mentioned studies could not be related to the mismatch between the

temporal and spatial scales encompassed by observations and models, with the local observations being used out of context with respect to the larger-scale GCM computations. One particular aspect in the systematic error in surface downward longwave radiation concerns the difference between the height at the location of the observations, and the model representation of the orography.

Chevallier and Morcrette (2000) recently compared the top-of-the-atmosphere (TOA) radiation produced by the 1998 version of the ECMWF model with CERES (Cloud and the Earth's Radiant Energy System) measurements for July 1998. They also compared monthly mean averaged diurnal cycle of downward radiation at the surface with surface observations. This study will concentrate on shorter time-scales (one hour to one day) and try to account for the problems linked to the various temporal/spatial scales. The longwave radiative fluxes, obtained during the first 36 hours of operational 10-day forecasts by the ECMWF forecast system, are compared to a variety of well calibrated surface radiation measurements (made as part of the Baseline Surface Radiation Network, BSRN (Ohmura et al., 1998), SURFace RADiation network, SURFRAD (1997), and Atmospheric Radiation Measurement programme, ARM (Stokes and Schwartz, 1994)). These measurements are available at a number of stations encompassing the various climatic regimes from polar to tropical latitudes. Working within the first few hours of the forecasts, when the model is still close to the analyzed initial conditions, should help pinpoint the reasons for discrepancies between model fields and observations. Also, such a study should reflect the evolution of the ECMWF model since the first ECMWF Re-Analysis (ERA-15: Gibson et al., 1997), which had been performed with the forecast system operational at the beginning of 1995.

The observational and model datasets used in this study are presented in section 2. Comparisons of operational surface radiation fields with observations are presented in section 3. The sensitivity of the surface radiation fields to details of the parametrization is presented in section 4. Discussion and conclusions are presented in section 5.

2. Data and methodology

2.1 Surface observations

The comparisons are made over 27 individual stations, which are part of either the BSRN, SURFRAD or ARM networks, and were operational over the months of April and May 1999. Figure 1 presents their geographical distribution, and Table 1 gives their characteristics. These stations span a large range of latitudes from high northern latitudes to the South Pole.

As discussed by Ohmura et al. (1998), the Baseline Surface Radiation Network aims at providing long-term measurements of the components of the surface radiation budget together with information on the relevant atmospheric profiles for a number of stations, each of them characteristic of a larger regional climate. Details on the required measurement accuracy and the methodology used to ensure that all measurements fulfill these requirements are given in Ohmura et al. (1998). The SURFace RADiation network (1997) is a collaborative effort among NOAA, NASA and U.S. university scientists. Locations were chosen with the intent of best representing the diverse climate of the United States, and special consideration was given to places where the landform and vegetation are homogeneous over an extended region so that the point measurements would be representative of a large area. The six stations presently available, although all continental in essence, encompass a wide range of atmospheric conditions, from the mountainous climate at Fort Peck, Montana to

the more humid climate of the Mississippi valley at Goodwin Creek. The Atmospheric Radiation Measurement program (Stokes and Schwartz, 1994) provides similar high-quality measurements of the surface radiation together with a wealth of information on the atmospheric structure through radiosonde, lidar, microwave radiometer and radar measurements. ARM data are available for the high-latitude site at Barrow (Alaska), two tropical Pacific sites (Nauru and Manus) and the mid-latitude South Great Plains site at Billings (Oklahoma).

All measuring stations used in this study have adopted the standards for measurement set by BSRN (WCRP, 1991; Heimo et al., 1993): These are 10 Wm^{-2} for broadband thermal infrared measurements. To achieve these goals, the broadband infrared instruments are calibrated against standards traceable to the World Radiation Centre in Davos, Switzerland. In a round-robin calibration experiment carried out within the BSRN stations, the calibrations of the set of pyrgeometers were shown (Philipona et al., 1998), over a two-year period, to be within 2 percent of the median, therefore within the 10 Wm^{-2} precision required for climate applications.

Most stations used in this study measure the downward and upward longwave radiation at the surface with a typical frequency of 0.3 Hz. The thermal infrared radiation is usually measured by an upward looking broadband pyrgeometer for downward longwave radiation, and another pyrgeometer is mounted facing downward, usually on a crossarm near the top of a 10-metre tower to measure the upwelling longwave radiation. These two measurements of upwelling and downwelling radiation in the infrared wavebands with their equivalent in the solar wavelengths constitute the complete surface radiation budget. Although all observations are made available with a frequency of at least 3 minutes, all parameters have been averaged over one hour intervals for comparisons with the model surface radiation fields. Given the generally large variability in observed surface temperature and emissivity due to surface type and vegetation varying over small distances, the model upwelling radiation over a model grid is usually difficult to compare to station measurements of the same quantity (Morcrette, 2001). As the focus is on comparing with radiation parameters operationally provided by the ECMWF forecast system, only the downward longwave radiation emitted by the atmosphere and available at the surface will be considered.

2.2 Conventional radiosonde and synoptic observations.

Table 1 also gives the coordinates of the stations where the radiosonde (RAOB) and synoptic (SYNOP) observations are used in the ECMWF operational analysis. The conventional meteorological observations have been extracted from the Global Telecommunication System over the study period for those RAOB and SYNOP sites closest to the radiation-measuring stations. Only a few sites have the radiation measurements exactly collocated with the radiosonde and synoptic observations. Therefore we selected radiosoundings from the geographically closest RAOB sites, and synoptic observations from SYNOP sites wich are the closest in terms of location (and height when several are within the same radius from the radiation-measuring station). For most of the locations considered in this study, the RAOB and SYNOP are within 10 to 20 kilometers from the location of the radiation measurements. Exceptions are Regina, Fort Peck, Carpentras, Penn State, Bondville, Boulder/Table Mountain, Goodwin Creek, Florianopolis, where the RAOB and SYNOP are usually within 100 kilometers of the radiation measurements. For Nauru, collocated RAOB and SYNOP are available as part of the ARM program, but the observations do not enter the ECMWF analysis system, as they are not available on a near real-time basis. Only Ilorin has both its corresponding radiosounding and synoptic observations more than 300 km away from the site of the radiation measurements.

2.3 Model data

All model data used in this study are taken from series of forecasts, starting 24 hours apart, between the 31 March 12 UTC and the 31 May 1999 12 UTC, run when preparing for the introduction of a new LW radiation scheme, the Rapid Radiation Transfer Model (Mlawer et al., 1997), into the ECMWF forecasting system. The analyses from which the forecasts were started are obtained through the operational 4DVAR, a four-dimensional variational assimilation of all the observations during a 6-hour window centered around the analysis time (Rabier et al., 1998; Mahfouf and Rabier, 2000).

The model used in this study is the so-called cycle 23R1 version of the ECMWF forecast system, operational between the end of June and mid-September 2000. This version differs significantly from the version used for ERA-15, the 15-year reanalysis (Gibson et al., 1997). A number of important model changes concern the horizontal and vertical resolution, now T_L319 (i.e., a grid of about $[0.5625\ ^o]^2$) and 60 vertical levels, instead of the T106 (i.e., $[1.125^o]^2$) and 31 vertical levels. The change in horizontal resolution was accompanied by a change in the model orography. The dynamical part of the model includes the two-time-level semi-lagrangian scheme on a linear grid (Temperton et al., 2001). Together with the spectral description of some of the dynamical fields, the ECMWF model has a reduced horizontal grid for all its grid-point computations, keeping roughly the same grid size (about 60 km) when going from equator to poles (Hortal and Simmons, 1991).

Most of the physics package has received some revision between the ERA-15 and cycle 23R1 versions of the ECMWF model. Particularly relevant to this study is the original version of the LW radiation scheme of Morcrette (1991) used for ERA-15, its revision in December 1997 (Gregory et al., 2000), and the present RRTM LW radiation code that became operational on 27 June 2000, and is now being used for ERA-40.

With respect to the clouds, the switching between deep or shallow convection was modified from a test on the moisture convergence to one based on the depth of the convection. Furthermore, the deep convective closure was changed from one based on moisture convergence (Tiedtke, 1989) to one that relates the convection to the reduction of the convective available potential energy (CAPE) towards zero over a certain timescale (Nordeng, 1994). The prognostic cloud scheme (Tiedtke, 1993) represents both stratiform and convective clouds, and their time evolution is defined through two large-scale budget equations for cloud water content and cloud fractional cover. This scheme links the formation of clouds to large-scale ascent, diabatic cooling, boundary-layer turbulence, and their dissipation to adiabatic and diabatic heating, turbulent mixing of cloud air with unsaturated environmental air, and precipitation processes. The results presented in the following sections are obtained with the scheme operationally used for global forecasts and analyses (Jakob, 1994) during the summer of 2000. It differs from Tiedtke's original formulation through a revised representation of the ice sedimentation after Heymsfield and Donner (1990) and through a new precipitation scheme (Jakob and Klein, 2000), which accounts for the overlap between cloud layers when computing the evaporation of the falling precipitation.

Together with the RRTM LW scheme, the model configuration used in Section 3 uses the cloud LW optical properties from Smith and Shi (1992) for liquid water clouds, and those from Ebert and Curry (1992) for ice water clouds. A fixed effective radius of 10 μm over land and 13 μm over the ocean is assumed for the liquid water cloud droplets. The effective particle dimension De varies between 30 and 60 μm for the ice particles, following the temperature dependence parametrization of Ou and Liou (1995) with provision made for the

precipitation of all ice particles with De larger than 60 μm (Jakob and Klein, 2000). Mixed phase clouds are considered between 0 and -23 ^{o}C following Matveev (1984). All optical thicknesses, before entering the radiative computations, are scaled by the 0.7 inhomogeneity factor according to Tiedtke (1996).

3. Comparison of operational surface radiation fields with observations

3.1 Discrepancy between model and actual orography

The first problem when comparing the model surface downward longwave radiation (SDLW) with observed SDLW, particularly in the framework of a large-scale numerical model of the atmosphere (with a spectral description for some of its prognostic fields) is the potential difference in orography between model and observations. When a difference in surface altitude between the measuring station and the model grid exists, it gives rise to an almost constant bias in surface pressure. Such a difference in surface pressure, Δp, is illustrated in Figure 2 for six stations (Ny Alesund, Boulder, and Florianopolis with a negative difference between model and station pressure, Barrow without any noticeable difference, and Alice Springs and South Pole with a positive difference in surface pressure). Based on the difference between the altitude at the observing station, Zs (given in Table 1 as station height), and the orography Zm in the corresponding model grid (given in Table 1 as model height), stations can be sorted in different categories: these for which Zm < Zs, i.e., Regina, Goodwin Creek, Ilorin, Alice Springs, Syowa, Georg von Neumayer, South Pole, these for which Zm equals to Zs within 10 m, i.e., Barrow, Bondville, Billings, Bermuda, Kwajalein, Nauru, Manus, and those for which Zm > Zs, i.e., Ny Alesund, Fort Peck, Budapest, Payerne, Carpentras, Penn State U, Table Mountain/Boulder, Desert Rock, Tateno, Florianopolis. In principle, in absence of other systematic errors, the model SDLW should be smaller than the observed one in the first case, about equal in the second case, and the model SDLW larger than the observed one in the last case. Wild et al. (1995a) used a height gradient of 2.8 Wm^{-2} $(100m)^{-1}$ to correct for the difference in height between model and observations. This correction factor had been derived from three stations at different heights in the Alps, part of the Swiss radiation network, and found to come very close to the gradient found in the Alps for the T106 model they were validating (3 Wm^{-2} $(100m)^{-1}$). Similar computations were repeated with the ECMWF model for all stations where model height Zm differs from the observing station height Zs by more than 10 m. Results appear in Table 2, for both the operational model, and for model fluxes corrected according to Wild et al. (1995). To investigate the effect of the different parameters on such a correction, calculations were also carried out including first an explicit correction on the surface pressure, based on the usually systematic difference in surface pressure between the model location and the pressure at the observing station, as illustrated in Figure 2. The results appear as Model +Δp in Table 2. Next calculations include corrections for both surface pressure and temperature, this last parameter interpolated/extrapolated from the original temperature profile based on the new pressure coordinate (Model+Δp+T, in Table 2). Finally, keeping the original profiles of relative humidity, calculations were repeated allowing for adjustments in pressure, temperature and specific humidity (Model+Δp+Tq, in Table 2). Overall, for clear-sky and total fluxes over a two-month period, the Δp+Tq correction is as successful as the W95 correction. However, on a one-hour basis, the Δp+Tq correction is more likely to be better adapted to more complex individual situations. An example is the South Pole where the Δp+Tq correction improves the model result as it can account for the effect of temperature inversions whereas W95 actually deteriorates the original model result.

For the following comparisons with observations, results are presented with the physically based Δp+Tq correction applied to the 16 stations in Table 2. Results for all other stations are given without correction.

3.2 Comparisons with observations

The one-hour time-series of the surface downward longwave radiation during the April-May 1999 period are presented in Figures 3 to 8 for 25 stations encompassing a very large range of climatic conditions: polar latitudes in Figure 3 (Ny Alesund and Barrow in the Northern hemisphere, and Syowa, Georg von Neumayer in the Southern hemisphere); mid-latitudes in Figures 4 to 6, sub-tropical (Bermuda, Alice Springs and Florianopolis) in Figure 7, and deep tropical latitudes (Kwajalein, Nauru and Manus over the West Pacific), in Figure 8. These stations also cover a large range of atmospheric humidity from the dry and cold high latitudes to the dry and warmer mid-latitude (Desert Rock and Alice Springs) to the moist tropical conditions over the West Pacific.

As seen from Figures 3 to 8, the model is generally successful at representing the intradiurnal and day-to-day variability of the atmosphere, with a usually good representation of the successive minima and maxima of the downward LW radiation. No station appears to display a behaviour systematically different from the observations. High-latitude stations (Figure 3) show the model to underestimate the high values, corresponding to cloudy events. Positive values of the difference Model-Observations correspond to the model producing low-level clouds when the observations are actually of clear-sky. For mid-latitude stations (Figures 4 to 6) including Florianopolis (Figure 7), the most striking difference is in the diurnal fluctuations, with the model usually displaying variations of a much larger amplitude than the observations (see particularly Desert Rock, Tateno). The overestimated amplitude can be linked to too low a minimum SDLW as in Budapest (first half of April), Carpentras (most of the period), Bondville, too large a maximum as in Penn State U (beginning of May), or to a combination of both as in Boulder, Desert Rock, Tateno, Florianopolis. Whereas, for these last five stations, the effect is somewhat enhanced by the large $\Delta p+Tq$ correction, the main signal is also present is the uncorrected field (not shown). The main reason for this excessive diurnal cycle in SDLW appears to be linked to too strong a connection of the planetary boundary-layer temperature to the surface conditions. For stations with overall clear-sky conditions (Boulder, Desert Rock), this problem is further enhanced during daytime by the known overestimation of the surface downward shortwave radiation by the current shortwave radiation scheme (Morcrette, 1991).

The agreement in SDLW for the few days of observations available for Bermuda (Fig. 7) is quite good. In the deep tropics over the West Pacific (Fig. 8), the average level of SDLW is well represented, but due to the large effect of the background water vapour absorption, it is rather difficult to judge the success of the model at representing the small amount of temporal variability linked to the variability in cloudiness.

The time-averages of the observed and model SDLW are presented in Table 3 for all stations when observations are present. Results are further separated between clear-sky and overcast conditions based on the model total cloud cover and the time evolution of the cloudiness in the synoptic reports.

Over the clear-sky situations available for each station over the two months, only Boulder and Ilorin presents an overestimation of the SDLW by more than 10 Wm^{-2}. The large $\Delta p+Tq$ correction for Boulder and the absence of nearby synoptic observation for Ilorin might explain these larger differences. All other stations are within 10 Wm^{-2}, with the model clear-sky SDLW generally smaller than the observed clear-sky SDLW. For overcast conditions, most stations are within 10 Wm^{-2}: Carpentras, Boulder, Tateno and Florianopolis show model values smaller than the observations by 16 to 23 Wm^{-2}. Part of the difference might be explained by the $\Delta p+Tq$ correction method, which does not affect the emitting temperature of the cloud base in the height

adjustment. Ilorin displays a 19 Wm^{-2} overestimation by the model in overcast conditions, consistent with the 17 Wm^{-2} overestimation in clear-sky conditions. The absence of a synoptic station close to the radiation-measuring site prevents from drawing any firm conclusion. Averaged over two months, without consideration for cloud conditions, the agreement between model and observations is within 10 Wm^{-2} for most stations. Only Barrow (-14 Wm^{-2}), Carpentras (-18 Wm^{-2}), Bondville (-14 $Wm^{-2)}$, Ilorin (+22 Wm^{-2}), Alice Springs (-17 Wm^{-2}) and South Pole (-13 Wm^{-2}) show higher levels of errors. However, these errors are much smaller than what was reported by Wild et al. (2001) for ERA-15, where errors for April and May were respectively -13 Wm^{-2} for Barrow, -4 Wm^{-2} for Payerne, -14 Wm^{-2} for Boulder, -18 Wm^{-2} for Tateno, +2 Wm^{-2} for Bermuda, +3 Wm^{-2} for Kwajalein, +12 Wm^{-2} for Ilorin, and -63 Wm^{-2} for Syowa, -11 Wm^{-2} for Georg von Neumayer and -34 Wm^{-2} for South Pole (see their Figure 8).

4. Sensitivity to modelling assumptions

The results presented in the previous section had been obtained with the operational representation of the physical processes in the ECMWF model as of Summer 2000. In the following, the surface radiation fluxes are studied in terms of their sensitivity to the various versions of the radiation codes available at ECMWF, and to the various representations of the aerosols and of the cloud optical properties. In the following, even if the physically based $\Delta p+Tq$ correction or the W95 correction would generally slightly improve the agreement with the observations, the results will be presented without any correction so as to show the real impact of the various modelling assumptions and to facilitate comparisons between different radiative configurations.

4.1 Radiation codes

Between May 1989 and December 1997, the LW radiative computations in the ECMWF model were carried out using the spectral emissivity method of Morcrette (1991; hereafter results with this version of the LW scheme are denoted M'91) and the shortwave radiative computations with the two-spectral interval version of the scheme by Fouquart and Bonnel (1980). Both parametrizations were using absorption coefficients derived from the HITRAN'86 spectroscopic database (Rothman et al., 1987) using a Malkmus statistical model to derive transmission functions for water vapour, uniformly mixed gases and ozone on a 0.01 μm basis, before doing the convolution with either the black-body functions or the spectral distribution of the solar energy (Morcrette et al., 1986). The parametrized transmissivities for H_2O, CO_2, O_3, N_20, CH_4 , were computed for the 6 spectral bands of the LW scheme. Cloud optical properties for both liquid and ice water clouds were taken from Smith and Shi (1992) and were available as emissivities over the whole LW spectrum. The liquid water cloud effective radius was varying between 10 μm at the surface and 45 μm at the top of the atmosphere, as a function of pressure. The ice particle radius was fixed to 40 μm. ERA-15 computations were performed with this version of the LW radiation scheme.

In December 1997, together with revision to other parts of the package of physical parametrizations (Gregory et al., 2000), most of the absorption coefficients for the water vapour lines, and the water vapour continuum coefficients were replaced following the approach by Zhong and Haigh (1995), using absorption coefficients derived from the HITRAN'92 spectroscopic database (Rothman et al., 1992). Furthermore, the ice cloud longwave optical properties were made consistent in both the longwave and shortwave parts of the spectrum, based on Ebert and Curry (1992). This revised scheme was operationally used in the ECMWF model from 17 December 1997 to 26 June 2000. Such an emissivity method has a quadratic dependence on the number of vertical levels. In the following, results with this version of the longwave scheme are denoted G'00.

With the increase in vertical resolution of the ECMWF model from 31 to 50 in September 1998 then to 60 levels in April 1999, a linear dependence on the number of vertical levels of the radiative computations was becoming necessary. The Rapid Radiation Transfer Model of Mlawer et al. (1997), being validated not only on line-by-line model results, but also on spectrally detailled measurements of the surface longwave radiation available as part of the ARM program, was tested within the ECMWF model and shown to have a positive impact on most aspects of the model (Morcrette et al., 1998). Contrary to the M'91/G'00 schemes., RRTM allows to deal with both the true cloud fraction and spectrally defined emissivities and transmissivities in each of the 16 different spectral bands. Since 27 June 2000, the ECMWF forecast system has been using RRTM for its LW computations. Also in June 2000, the spectral resolution of the SW radiation scheme was changed from two spectral intervals (0.25-0.69-4.00 μm) to four spectral intervals (0.25-0.69-1.19-2.38-4.00 μm).

Table 4 compares the SDLW averaged over the two months of April and May 1999, for all one-hour slots within the two months and for those situations given as clear-sky by the model, computed with the M'91, G'00 and RRTM LW schemes. All computations are made from the same fields with the 60-level vertical resolution. No provision is made for inhomogeneity effect in any of these computations. Considering first the clear-sky situations, M'91 and G'00 SDLWs are generally within 1 or 2 Wm^{-2} from each other, showing the strong relationship between the two versions of the codes. By contrast, SDLW provided by RRTM is systematically higher by 1 to 2 Wm^{-2} at high latitudes, by 3 to 6 W m^{-2} at low latitudes. This possibly reflects the use of a more recent spectroscopic database (HITRAN'96: Rothman et al., 1996), but more certainly the better handling of the water vapour absorption, by both the lines and the continuum in RRTM. When clouds are considered, G'00 are generally lower than M'91, reflecting both the impact seen in clear-sky conditions and the fact that, for the same ice cloud water content, the ice cloud emissivity produced by Smith and Shi (1992) (used in M'91 and ERA-15) is higher than that produced by Ebert and Curry (1992) (used in G'00). When RRTM is considered (with Ebert and Curry's ice cloud optical properties), SDLW are systematically higher than either G'00 or M'91, by 1 to 7 Wm^{-2}.

4.2 Cloud optical properties

In the ECMWF radiation scheme operational as of summer 2000, the water cloud optical properties are defined from Smith and Shi (1992) in the LW, and Fouquart (1987) in the SW. The effective radius for water cloud droplets is specified as 10 μm over land and 13 μm over the ocean. For ice clouds, optical properties are taken from Ebert and Curry (1992) in both the LW and SW. Effective particle size De varies between 30 and 60 μm (see section 3). In Tables 5 to 9, the SDLW is presented averaged over the two months of April and May 1999, for all one-hour slots within the two months and separately for all overcast situations occurring over these two months. Overcast situations are diagnosed from the model total cloudiness being larger than 0.99. All computations are done with the RRTM LW radiation scheme, but differ through the choice of cloud optical properties, cloud effective particle size, and cloud inhomogeneity treatment.

Table 5 illustrates the impact of various specifications of the optical properties of liquid water clouds. For Smith and Shi (1992; SS'92), the liquid water cloud LW emissivity is diagnosed for the whole LW spectrum from the liquid water path (LWP). For Savijarvi and Raisanen (1997; SR'97) and Lindner and Li (2000; LL'00), it is diagnosed for each of the 16 spectral intervals of RRTM. When the liquid water clouds are the lowest ones in the atmospheric column and the liquid water content is large enough to make the clouds radiatively black, the impact of different representations of the mass absorption coefficient is small, typically smaller than 1 Wm^{-2}. It is only for the high latitudes (NYA, BAR, SYO, GVN) that the liquid water content is

small enough for the emissivity to differ significantly from unity, in which case, the impact of the different formulations becomes apparent.

The sensitivity of SDLW to various representations of the optical properties of ice water clouds is shown in Table 6. For SS'92, the ice water cloud LW emissivity is diagnosed for the whole LW spectrum from the ice water path. For EC'92, Fu and Liou (1993; FL'93) and Fu et al. (1998; Fu'98), the spectral mass absorption coefficients given by the different authors are interpolated to the 16 spectral intervals of RRTM. Again, when the lowest cloud layers are made of liquid water with the resultant cloud emissivity at or close to saturation, the impact of different representations of the ice cloud optical properties is small, typically smaller than 2 Wm^{-2}. At high latitudes (NYA, BAR, SYO, GVN, SPO), or somewhat over high grounds (BOU), the change in ice cloud optical properties induces variations between 2 and 6 Wm^{-2} on SDLW averaged over two months, going to 9 Wm^{-2} for SPO.

The impact on SDLW of different specifications of the effective radius Re of the droplets in liquid water clouds appears in Table 7. *f(P)* refers to the formulation originally used for ERA-15, where Re varies from 10 μm at the surface to 45 μm at the top of the atmosphere as a linear function of pressure, *fixed* refers to 10 μm droplets over land and 13 μm droplets over the oceans, and *M'94* is the diagnostic formulation of Martin et al. (1994). Averaged over two months, the impact is negligible, as even when Re is diagnosed (Martin et al., 1994), the resulting Re is usually smaller than the specified values, which leads to higher optical thickness, of no impact on an already saturated cloud emissivity. For high latitude stations, only when looking at individual hours, can any impact, always smaller than 2 Wm^{-2}, be found.

The change in SDLW linked to the representation of the effective dimension of the particles in ice clouds is given in Table 8. 40 refers to the particle size used for ERA-15, where all ice particles have a De of 40 mm. 40-130 and 30-60 refer to the temperature-dependent formulation of Ou and Liou (1995), with the two figures giving the range of variations for De. S'01 refers to the diagnostic formulation of Sun (2001), which relates De to both the temperature and the ice water content in the cloud. The effect of a different representation of De is very similar to what was found for a different representation of the ice cloud optical properties. Largest impact is found at high latitudes, particularly for the South Pole (Figure 9) where a diagnosed De from temperature and ice water content allows to correct a large fraction of the underestimation compared to observations.

Table 9 presents, for the set of parametrizations presently used in the ECMWF model, the impact of the 0.7 inhomogeneity factor that has been introduced in June 2000 in the longwave radiative computations of the operational ECMWF model. Overall, the inhomogeneity factor only has a small impact (< 1 Wm^{-2}) on the two-month averages of the SDLW for middle and low latitudes. At high latitudes (NYA, BAR, SYO, GVN, SPO), its effect is similar to an increase in Re and De, i.e., a decrease in SDLW.

4.3 Representation of aerosols

The ECMWF model is operationally run with an annually averaged climatological distribution of aerosols, originally designed by Tanre et al. (1983). In the present model configuration, five types of aerosols are considered, four with a geographical variation (maritime, continental, urban and desert aerosols), the fifth one, a stratospheric background aerosol, is included with a homogeneous horizontal distribution. This representation of aerosols is referred to as AER1 in the following. Recently, the distribution of tropospheric

aerosols derived from a chemical transport model by Koepke et al. (1997) and Hess et al. (1998) was adapted to the ECMWF model. This new climatology is given as monthly mean distributions of optical thickness, asymmetry factor, and single scattering albedo for sea salt aerosol, sulfate aerosol, soil dust aerosol, organic aerosol and black carbon aerosol. They have been given the same vertical distributions as the previous climatology, and obviously impact only the troposphere. This new aerosol climatology is referred to as AER2.

Table 10 compares for all stations the SDLW computed without accounting for any aerosol effect, and with the operational AER1 and new AER2 geographical distributions and sets of optical properties for the aerosols. As expected, in the longwave part of the spectrum, the aerosol effect on the surface downward longwave radiation remains small (< 2 Wm^{-2}), with the impact of the revised climatology even smaller.

5. Discussion and concluding remarks

In this study, two sets of questions have been addressed: Firstly, what is the quality of the surface longwave radiation fluxes produced by a version of the ECMWF forecast system very similar to the one presently used for the 40-year reanalysis, and will the ERA-40 surface longwave radiation fluxes be better than those available as part of ERA-15, as judged by comparisons with observed fluxes. Secondly, using a series of sensitivity studies and assuming the cloud information to be specified by the ECMWF model analysis, what is the potential for improving the SDLW through different choices in the representation of the cloud optical properties, of the cloud effective particle size, of the aerosols. A related question is how sensitive the SDLW is to various specifications of cloud parameters, presently out of the scope of a representation by prognostic equations in GCMs.

To answer these questions, the surface downward longwave radiation produced by a recent version of the ECMWF model has been compared to high-quality measurements at 25 sites covering the entire latitude range, over the months of April and May 1999. Comparisons have been done on a one-hour basis, in an attempt at separating clear-sky and overcast situations from those with a partial cloudiness in the column over the sites. Looking first at the clear-sky situations, the present version of the ECMWF model, including the RRTM longwave scheme is shown to be in a generally good agreement with the observations, with the discrepancies likely to be mainly linked to errors in the model definition of the temperature and humidity profiles. For overcast profiles, the agreement between model and observations is also generally good, showing the model essentially produced clouds with their base at the proper height. When all cases are considered, errors are usually larger, reflecting some deficiencies in the model timing in its production of cloudiness. However, the version of the model used here improves the surface downward longwave fluxes relative to the ERA-15 fluxes. The ERA-40 system is running with a different resolution (TL159 instead of the TL319 of this study), and the analysis is carried out with a three-dimensional variational (3DVAR) system instead of the operational 4-DVAR used here. However, on pointwise comparisons over the first hours of the forecasts, at points where radiosonde and synoptic observations are usually available, 3DVAR forecasts of a vertically integrated quantity like SDLW should be similar in behaviour to 4DVAR forecasts, so the results presented here should augur of the quality of the final ERA-40 SDLW.

A proper surface energy budget over land should be linked to a proper determination of each of the radiative and turbulent components. This study shows how the downward longwave radiation is behaving. In particular, the comparisons in Section 3 show the rather correct forcing by the (low-level) clouds produced by the prognostic cloud scheme, inducing a realistic modulation of the SDLW.

Computations have also been carried out to test the sensitivity of the surface downward longwave fluxes to most of the parameters usually specified in a longwave radiation parametrization. Profiles from only one set of assimilations were used, so results presented here do not include potential feedbacks that the various changes could have brought to the SDLW. A complete study would have involved numerous sets of two-month long assimilations. However, results from the sensitivity study of Section 4 represent the first-order impact of what could be expected from a fully interactive system.

For SDLW, the formulation chosen for the cloud optical properties of liquid water clouds is not critical, as the cloud liquid water path generally leads to an emissivity of one. Similarly, the definition of the effective radius of the liquid water droplets is shown to have a marginal effect on the SDLW. Only at high latitudes, where the cloud water path is small enough for the cloud emissivity to differ from unity, can differences reach 2 Wm^{-2}. The choice of the ice cloud optical properties introduces a larger sensitivity particularly for high latitudes. The present model formulation using ice cloud optical properties from Ebert and Curry (1992) and an effective particle diameter De simply diagnosed from temperature fails to capture the full effect of clouds on the surface downward longwave radiation of the polar latitudes. A diagnostic of De from both temperature and ice water content, such as recently proposed by Sun (2001), corrects most of the underestimation in SDLW. As any change which decreases the cloud optical thickness, the 0.7 inhomogeneity factor of Tiedtke (1996) has little effect on the SDLW outside the arctic and antarctic regions. As expected, the aerosols play a small role on the SDLW (up to +1 Wm^{-2} compared to calculations without aerosols).

In conclusion, from the comparisons of model SDLW with observations and the sensitivity calculations, only the radiative parametrizations related to ice clouds show a potential for further improvement of the ECMWF surface downward longwave radiation. Improvements might also be brought by a better representation of the time evolution of the cloudiness.

Acknowledgments:

Dr E. Dutton, B. Forgan, H. Hegner, A. Heimo, G. Koenig-Langlo, G. Major, B. McArthur, R. Pinker, and T. Yamanouchi are gratefully acknowledged for providing BSRN-type data prior to their compilation in the official BSRN database. The SURFRAD data were downloaded from the SURFRAD web site and Dr John Augustine was very helpul in answering my questions. Thanks to Robin Perez for help in acquiring the ARM observational data and pointing to the relevant documentation. The Atmospheric Radiation Measurement (ARM) Program is sponsored by the U.S. Department of Energy, Office of Science, Office of Biological and Environmental Research, Environmental Sciences Division. Dr M. Wild provided insight in the comparisons between observations and ERA-15. At ECMWF, the continuous help of Dominique Lucas in dealing with the various observation file formats was greatly appreciated. I am most grateful to Anders Persson, Pedro Viterbo and Anton Beljaars for help in dealing with the RAOB and SYNOP information stored in the ECMWF archiving system. Drs Martin Miller. Anton Beljaars, and Frederic Chevallier are thanked for their comments on an earlier version of the manuscript.

References

Chevallier, F., and J.-J. Morcrette, 2000: Comparison of model fluxes with surface and top-of-the-atmosphere observations. Mon. Wea. Rev., 128, 3839-3852.

Darnell, W.L., S.K. Gupta, and W.F. Staylor, 1983: Downward longwave radiation at the surface from satellite measurements. J. Clim. Appl. Meteorol., 22, 1956-1960.

Darnell, W.L., W.F. Staylor, S.K. Gupta, N.A. Ritchey, and A.C. Wilber, 1992: Seasonal variation of surface radiation budget derived from ISCCP-C1 data. J. Geophys. Res., 97D, 15741-15760.

Ebert, E.E., and J.A. Curry, 1992: A parameterization for ice optical properties for climate models. J. Geophys. Res., 97D, 3831-3836.

Fouquart, Y., 1987: Radiative transfer in climate models. NATO Advanced Study Institute on Physically-Based Modelling and Simulation of Climate and Climatic Changes. Erice, Sicily, 11-23 May 1986. M.E. Schlesinger, Ed., Kluwer Academic Publishers, 223-284.

Fouquart, Y., and B. Bonnel, 1980: Computations of solar heating of the earth's atmosphere: a new parameterization. *Beitr. Phys. Atmosph*., 53, 35-62.

Fu, Q., and K.-N. Liou, 1993: Parameterization of the radiative properties of cirrus clouds. J. Atmos. Sci., 50, 2008-2025.

Fu, Q., P. Yang, and W.B. Sun, 1998: An accurate parameterization of the infrared radiative properties of cirrus clouds of climate models. J. Climate, 11, 2223-2237.

Garratt, J., P. Krummel, and E. Kowalczyk, 1993: The surface energy balance at local and regional scales: A comparison of general circulation model results with observations. J. Climate, 6, 1090-1109.

Garratt, J.R., A.J. Prata, 1996: Downwelling longwave fluxes at continental surfaces - A comparison of observations with GCM simulations and implications for the global land-surface radiation budget. J. Climate, 9, 646-655.

Garratt, J.R., A.J. Prata, L.D. Rotstayn, B.J. McAvaney, and S. Cusack, 1998: The surface radiation budget over oceans and continents. J. Climate, 11, 1951-1968.

Gibson, J.K., P. Kallberg, S. Uppala, A. Nomura, A. Hernandez, E. Serrano, 1997: The ECMWF Re-Analysis: ERA Description. ECMWF Re-Analysis Project Report Series, 1.

Gregory, D., J.-J. Morcrette, C. Jakob, A.C.M. Beljaars, and T. Stockdale, 2000 : Revision of convection, radiation and cloud schemes in the ECMWF Integrated Forecasting System. Quart. J. Roy. Meteor. Soc., 126, 1685-1710.

Gupta, S.K., A.C. Wilber, W.L. Darnell, and J.T. Suttles, 1993: Longwave surface radiation over the globe from satellite data: An error analysis. Intern. J. Remote Sensing, 14, 95-114.

Gupta, S.K., N.A. Ritchey, A.C. Wilber, C.H. Whitlock, G.G. GIbson, and P.W. Stackhouse, Jr., 1999: A climatology of surface radiation budget derived from satellite data. J. Climate, 12, 2691-2710.

Heimo, A., A. Vernez, and P. Wasserfallen, 1993: Baseline Surface Radiation Network (BSRN). Concept and implementation of a BSRN station. WMO/TD No. 579, WCRP/WMO, Geneva.

Heymsfield, A.J., and L.J. Donner, 1990: A scheme for parameterizing ice–cloud water content in general circulation models. J. Atmos. Sci., 47, 1865–1877.

Hess, P. Koepke, and I. Schult, 1998: Optical properties of aerosols and clouds: The software package OPAC. Bull. Amer. Meteor. Soc., 79, 831-844.

Hortal, M., and A.J. Simmons, 1991: Use of reduced Gaussian grids in spectral models. Mon. Wea. Rev., 119, 1057-1074.

Hortal, M., 1998: TL319 resolution and revised orographies. ECMWF Research Department Memorandum, R60.5/MH/23, 9 March 1998, 18 pp.

Hortal, M., 2000: The development and testing of a new two-time-level semi-Lagrangian scheme (SETTLS) in the ECMWF forecast model. Quart. J. Roy. Meter. Soc., in press.

Jakob, C., 1994: The impact of the new cloud scheme on ECMWF's Integrated Forecasting System (IFS). Proceedings of ECMWF/GEWEX Workshop on Modelling, Validation and Assimilation of Clouds, 31 October-4 November 1994, 277-294.

Jakob, C., and S.A. Klein, 2000: A parametrization of the effects of cloud and precipitation overlap for use in general circulation models. Quart. J. Roy. Meteor. Soc., 126C, 2525-2544.

Koepke, P., M. Hess, I. Schult, and E.P. Shettle, 1997: Global aerosol data set, GADS. Max-Planck-Institute Report No. 243, 44pp.

Lindner, T.H., and J. Li, 2000: Parameterization of the optical properties for water clouds in the infrared. J. Climate, 13, 1797-1805.

Mahfouf, J.-F., and F. Rabier, 2000: The ECMWF operational implementation of four dimensional variational assimilation: Part II: Experimental results with improved physics. Quart. J. Roy. Meteor. Soc., 126A, 1171-1190.

Martin, G.M., D.W. Johnson, and A. Spice, 1994: The measurement and parameterization of effective radius of droplets in warm stratocumulus. J. Atmos. Sci., 51, 1823-1842.

Matveev, L.T., 1984: Cloud Dynamics, D. Reidel Publish. Co., 340 pp.

Mlawer, E.J., S.J. Taubman, P.D. Brown, M.J. Iacono, and S.A. Clough, 1997: Radiative transfer for inhomogeneous atmospheres: RRTM, a validated correlated-k model for the longwave. J. Geophys. Res., 102D, 16,663-16,682.

Morcrette, J.-J., 1991: Radiation and cloud radiative properties in the ECMWF operational weather forecast model. J. Geophys. Res., 96D, 9121-9132.

Morcrette, J.-J., 2001: Assessment of the ECMWF model cloudiness and surface radiation fields at the ARM-SGP site. Mon. Wea. Rev., accepted for publication.

Morcrette, J.-J., S.A. Clough, E.J. Mlawer, and M.J. Iacono, 1998: Impact of a validated radiative transfer scheme, RRTM, on the ECMWF model climate and 10-day forecasts. ECMWF Technical Memo. No. 252, 47 pp.

Morcrette, J.-J., L. Smith, and Y. Fouquart, 1986: Pressure and temperature dependence of the absorption in longwave radiation parameterizations. Beitr. Phys. Atmosph., 59, 455-469.

Nordeng, T.E., 1994: Extended versions of the convection parametrization scheme at ECMWF and their impacts upon the mean climate and transient activity of the model in the tropics. ECMWF Tech. Memo. No. 206, pp.

Ohmura, A., E.G. Dutton, B. Forgan, C. Frohlich, H. Gilgen, H. Hegner, A. Heimo, G. Konig-Langlo, B. McArthur, G. Muller, R. Philipona, R. Pinker, C.H. Whitlock, K. Dehne, and M. Wild, 1998: Baseline Surface Radiation Network (BSRN/WCRP): New precision radiometry for climate research. Bull. Amer. Meteor. Soc., 79, 2115-2136.

Ou, S.C., and K.-N. Liou, 1995: Ice microphysics and climatic temperature feedback. Atmosph. Research, 35, 127-138.

Philipona, R., C. Frohlich, K. Dehne, J. DeLuisi, J. Augustine, E. Dutton, D. Nelson, B. Forgan, P. Novotny, J. Hickey, S.P. Love, S. Bender, B. McArthur, A. Ohmura, J.H. Seymour, J.S. Foot, M. Shiobara, F.P.J. Valero, and A.N. Strawa, 1998: The Baseline Surface Radiation Network pyrgeometer round-robin calibration experiment. J. Atmos. Ocean. Technol., 15, 687-696.

Rabier, F., J.-N. Thepaut, and P. Courtier, 1998: Extended assimilation and forecasts experiments with a four dimensional variational assimilation system. Quart. J. Roy. Meteor. Soc., 124, 1861-1887.

Rossow,W.B., and Y.-C. Zhang, 1995: Calculation of surface and top of the atmosphere radiative fluxes from physical quantities based on ISCCP data sets, 2: Validation and first results. J. Geophys. Res., 100, 1167-1198.

Rothman, L.S., R.R. Gamache, A. Goldman, L.R. Barrow, R.A. Toth, H.M. Pickett, R.L Poynter, J.-M. Flaud, C. Camy-Peyret, A. Barbe, N. Husson, C.P. Rinsland, and M.A.H. Smith, 1987: The HITRAN database: 1986 edition. Appl. Opt., 26, 4058-4097.

Rothman, L.S., R.R. Gamache, R.H. TIpping, C.P. Rinsland, M.A.H. Smith, D.C. Benner, V. Malathy Devi, J.-M. Flaud, C. Camy-Peyret, A. Perrin, A. Goldman, S.T. Massie, L.R. Brown, and R.A. Toth , 1992: The HITRAN database: Editions of 1991 and 1992. J. Quant. Spectros. Radiat. Transfer, 48, 469-507.

Rothman, L.S., C.P. Rinsland, A. Goldman, S.T. Massie, D.P. Edwards, J.-M. Flaud, A. Perrin, C. Camy-Peyret, V. Dana, J.-Y. Mandin, J. Schroeder, A. McCann, R.R. Gamache, R.B. Watson, K. Yoshino, K.V. Chance, K.W. Jucks, L.R. Brown, V. Nemtchinov, and P. Varanasi, 1996: HITRAN molecular database: Edition ’96. J. Quant. Spectros. Radiat. Transfer, 60, 665-710.

Stokes, G.M., and S.E. Schwartz, 1994: The Atmospheric Radiation Measurement (ARM) Program: Programmatic background and design of the cloud and radiation testbed. Bull. Amer. Meteor. Soc., 75, 1201-1221.

Savijarvi, H., and P. Raisanen, 1997: Long-wave optical properties of water clouds and rain. Tellus, 50A, 1-11.

Sun, Z., 2001: Reply to comments by G.M. McFarquhar on "Parametrization of effective sizes of cirrus-cloud particles and its verification against observations". Quart. J. Roy. Meteor. Soc., 127A, 267-271.

Tanre, D. J.-F. Geleyn, and J. Slingo, 1984: First results of the introduction of an advanced aerosol-radiation interaction in the ECMWF low resolution global model. in Aerosols and Their Climatic Effects, H.E. Gerber and A. Deepak, Eds., A. Deepak Publ., Hampton, Va., 133-177.

Temperton, C., M. Hortal, and A. Simmons, 2001: A two-time-level semi-Lagrangian global spectral model. *Quart. J. Roy. Meteor. Soc.*, 127A, 111-127.

Tiedtke, M., 1989: A comprehensive massflux scheme for cumulus parameterization in large scale models. Mon. Wea. Rev., 117, 1779-1800.

Tiedtke, M., 1993: Representation of clouds in large–scale models. Mon. Wea. Rev., 121,3040–3061.

Tiedtke, M., 1996: An extension of cloud-radiation parameterization in the ECMWF model: The representation of sub-grid scale variations of optical depth. Mon. Wea. Rev., 124, 745-750.

WCRP-54, 1991: Radiation and Climate: Workshop on the Implementation of the Baseline Surface Radiation Network. Washington, DC, 3-5 December 1990. WCRP Report No. 406, World Meteorological Organization, Geneva, Switzerland.

Wild, M., 1999: Discrepancies between model-calculated and observed shortwave absorption in Equatorial Africa. J. Geophys. Res., 104D, 27361-27371.

Wild, M., A. Ohmura, H. Gilgen, J.-J. Morcrette, and A. Slingo, 2001: Evaluation of the downward longwave radiation in general circulation models. J. Climate, accepted.

Wild, M., A. Ohmura, H. Gilgen, E. Roeckner, 1995a: Validation of general circulation model radiative fluxes using surface observations. J. Climate, 8, 1309-1324.

Wild M., Ohmura A., Gilgen H. and Roeckner E., 1995b Regional climate simulation with a high reslution GCM: surface radiative fluxes. Climate Dynamics, 11, p. 469-486.

Zhong, W, and J.D. Haigh, 1995: Improved broadband emissivity parameterization for water vapor cooling rate calculations. J. Atmos. Sci., 52, 124-138.

Electronic References

The AErosol RObotic NETwork, 2000: http://aeronet.gsfc.nasa.gov:8080/

The Atmospheric Radiation Measurement program, 1995: http://www.arm.gov

The Baseline Surface Radiation Network, 1999: http://bsrn.ethz.ch

The SURFRAD Network, 1997: http://www.srrb.noaa.gov/surfrad.htm

Station	Station index	latitude	longitude	height (m)	Model height (m)	Network	ID and coordinates of closest RAOB	closest SYNOP	SYNOP height (m)
Ny Alesund	NYA	78.93 N	11.93 E	11	107	BSRN	01004: 78.92N ; 11.93E	01007: 78.92N ; 11.93E	12
Barrow, AL	BAR	71.32 N	156.61 W	8	2	BSRN/ARM	70026: 71.30N ; 156.78W	70026: 71.30N ; 156.78W	4
Regina	REG	50.12 N	104.72 W	594	583	BSRN	71867: 53.97N ; 101.10W	71823: 50.43N ; 104.67W	577
Fort Peck, MT	FPK	48.31 N	105.10 W	634	726	SURFRAD	72768: 48.22N ; 106.62W	72767: 48.18N ; 103.63W	581
Budapest	BUD	47.83 N	19.05 E	139	192	BSRN	12843: 47.43N ; 19.18E	12844: 47.35N ; 18.98E	104
Payerne	PAY	46.82 N	6.95 E	491	590	BSRN	06610: 46.82N ; 6.95E	06610: 46.82N ; 6.95E	491
Carpentras	CAR	44.05 N	5.05 E	100	437	BSRN	07481: 45.73N ; 5.08E	07481: 45.73N ; 5.08E	240
Penn State Univ., PA	PSU	40.72 N	77.93 W	376	475	SURFRAD	72528: 42.93N ; 77.47W	72513: 41.33N ; 75.73W	289
Table Mountain, CO	TBM	40.13 N	105.24 W	1689	2544	SURFRAD	72469: 39.78N ; 104.87W	72469: 39.78N ; 104.87W	1626
Bondville, IL	BON	40.05 N	88.37 W	213	213	SURFRAD	74560: 40.15N ; 89.33W	72532: 40.67N ; 89.68W	202
Boulder, CO	BOU	40.05 N	105.01 W	1584	2544	BSRN	72469: 39.78N ; 104.87W	72565: 39.87N ; 104.67W	1656
Desert Rock, NV	DRN	36.63 N	116.02 W	1007	1447	SURFRAD	72387: 36.62N ; 116.02W	72387: 36.62N ; 116.02W	1009
Billings, OK	SGP	36.53 N	97.45 W	317	321	BSRN/ARM	72357: 35.22N ; 97.45W	72450: 37.65N ; 97.43W	409
Tateno	TAT	36.05 N	140.13 E	25	267	BSRN	47646: 36.05N ; 140.13E	47648: 35.73N ; 140.87E	28
Goodwin Creek, MS	GWN	34.25 N	89.87 W	98	83	SURFRAD	72340: 34.83N ; 92.25W	72332: 34.27N ; 88.77W	110
Bermuda	BER	32.30 N	64.75 W	1	0	BSRN	78016: 32.37N ; 64.68W	78016: 32.37N ; 64.68W	6
Kwajalein	KWA	8.71 N	167.73 E	10	0	BSRN	91366: 8.73N ; 167.73E	91366: 8.73N ; 167.73E	8
Ilorin	ILO	8.32 N	4.34 E	350	231	BSRN	64910: 4.02N ; 9.70E	65125: 9.25N ; 7.00E	344
Nauru	NAU	0.52 S	166.92 E	4	0	ARM	91610: 1.35N ; 172.92E	91533: 0.90S ; 169.53E	66
Manus	MAN	2.07 S	147.43 E	4	1	ARM	92044; 2.07S ; 147.43E	92044: 2.07S ; 147.43E	5
Alice Springs	ALS	23.70 S	133.87 E	547	440	BSRN	94326: 23.80S ; 133.88E	94326: 23.80S ; 133.88 E	546
Florianopolis	FLO	27.58 S	48.52 W	11	396	BSRN	83840: 25.52S ; 49.17W	83899: 27.67S ; 48.55W	5
Syowa	SYO	69.00 S	39.58 E	21	6	BSRN	89532: 69.00S ; 39.58E	89532: 69.00S ; 39.58E	21
Georg von Neumayer	GVN	70.39 S	8.15 W	42	2	BSRN	89002: 70.67S ; 8.25W	89002: 70.67S ; 8.25W	50
South Pole	SPO	90.00 S	0 .00	2841	2705	BSRN	89009: 90.00S ; 0.00	89009: 90.00S ; 0.00	2835

Table 1: Characteristics of the radiation, and conventional radiosonde and synoptic observation stations used in the study.

Stations are listed from North to South. Note latitude and longitude are given in degrees with decimals.

Station	Nclear	Clear-sky Obs	Clear-sky Model	Model +W95	Model +Δp	Model +Δp,T	Model +Δp,Tq	Ntot	Total sky Obs	Total sky Model	Model +W95	Model +Δp,Tq
NYA	11	203.1	195.5	198.2	196.3	197.1	197.4	1457	246.3	233.7	236.4	236.8
REG	132	252.9	249.6	249.3	249.6	249.6	249.6	1423	293.6	291.3	291.0	291.0
FPK	228	266.1	258.3	260.9	259.2	256.5	258.3	1464	295.9	291.7	294.3	293.8
BUD	134	281.9	269.3	270.8	269.7	270.8	271.4	1446	322.1	315.5	315.9	316.1
PAY	58	293.9	283.0	285.8	283.6	283.8	284.2	1424	326.1	321.1	323.9	322.6
CAR	32	307.1	295.5	304.9	298.4	301.1	300.9	1464	340.8	316.1	330.5	322.8
PSU	312	266.0	258.7	261.5	259.9	259.8	261.7	1460	312.7	306.8	309.6	311.3
BOU	14	227.7	216.6	243.5	222.1	238.4	244.3	1464	293.8	257.8	284.7	300.5
DRN	210	275.9	256.8	269.1	260.1	267.0	273.6	1456	295.1	277.5	289.8	296.0
TAT	57	299.4	284.4	291.2	285.9	287.6	288.0	1397	345.5	330.3	337.1	336.0
GWN	276	312.2	306.8	306.4	306.8	306.7	306.8	1464	356.5	356.6	356.5	356.6
ALS	410	303.6	298.2	295.2	297.4	296.0	294.8	1415	322.4	307.0	304.0	305.9
FLO	21	310.5	300.6	310.7	303.5	315.5	316.6	1450	379.3	357.7	360.7	372.0
SYO	35	166.7	150.9	150.5	150.8	150.8	150.9	1453	233.1	213.2	212.8	213.1
GVN	33	149.9	149.1	148.0	148.8	149.9	149.5	1456	201.0	201.8	200.7	201.4
SPO	40	77.7	74.3	70.5	74.1	76.7	77.0	1400	102.0	83.6	79.8	88.7

Table 2: Impact of different orography corrections on the surface clear-sky and total downward longwave radiation

Nclear and Ntot are the number of clear-sky and total sky one-hour comparisons possible over a given site over the April-May 1999 period. W95 refers to the 2.8 Wm-2 (100m)-1 correction factor of Wild et al. (1995a). Δp includes an adjustment of the pressure levels based on the difference between model and surface pressure, T includes a temperature interpolation/extrapolation based on the adjusted pressure distribution, q includes an adjustment to the specific humidity based on a fixed relative humidity when T is adjusted.

Station	Total			Clear-sky			Overcast		
	Ntot	Obs	Model	Nclear	Obs	Model	Novcst	Obs	Model
NYA	1457	246.3	236.8	11	203.1	197.4	165	275.5	277.1
BAR	1464	225.0	211.0	131	188.1	192.6	174	246.6	246.6
REG	1423	293.6	291.0	132	252.9	249.6	n/a	n/a	n/a
FPK	1464	295.9	293.8	228	266.1	258.3	287	314.9	316.1
BUD	1446	322.1	316.1	134	281.9	271.4	156	346.7	346.7
PAY	1424	326.1	322.6	58	293.9	284.2	303	340.6	345.4
CAR	1464	340.8	322.8	32	307.1	300.9	220	360.5	344.7
PSU	1460	312.7	311.3	312	266.0	261.7	152	348.8	346.8
BOU	1464	293.8	300.5	14	227.7	244.3	222	323.0	303.9
BON	1464	345.9	332.4	219	300.1	286.8	233	367.8	359.8
DRN	1456	295.1	296.0	210	275.9	273.6	99	307.8	303.8
SGP	1436	341.3	339.4	168	294.1	292.2	59	357.5	359.3
TAT	1397	345.5	336.0	57	299.4	288.0	372	375.7	359.4
GWN	1464	356.5	356.6	276	312.2	306.8	139	382.7	387.9
BER	464	375.9	372.3	7	348.8	341.7	16	388.1	402.5
KWA	1464	416.5	416.2	0	n/a	n/a	420	417.3	417.8
ILO	719	396.5	418.8	53	392.7	409.2	68	398.2	417.4
NAU	1387	414.9	416.7	0	n/a	n/a	319	417.6	418.3
MAN	1294	421.2	430.3	0	n/a	n/a	507	423.6	423.3
ALS	1415	322.4	305.9	410	303.6	294.8	60	344.2	337.8
FLO	1450	379.3	372.0	21	310.5	316.6	107	407.2	384.2
SYO	1453	233.1	213.1	35	166.7	150.9	743	246.2	239.9
GVN	1456	201.0	201.4	33	149.9	149.5	461	233.1	249.1
SPO	1400	102.0	88.7	40	77.7	77.0	1108	105.4	86.0

Table 3: Comparison of operational ECMWF surface downward longwave radiation with observations.

Comparisons are made for all slots for which observations are available during the full hour. All model results include the $\Delta p+Tq$ orographic correction when relevant. Clear-sky (overcast) situations are defined as the situations within 3 hours of a synoptic observation reporting no cloudiness (total cloudiness: 8 octas) and for which the model total cloudiness is lower than 5 percent (larger than 99 percent). SGP results are for the E13 station. All surface downward longwave (SDLW) fluxes are in Wm^{-2} and correspond to resulst for April-May 1999.

Station	Radiation Code					
	Clear-sky			Total		
	M'91	G'00	RRTM	M'91	G'00	RRTM
NYA	211.9	211.8	213.9	235.9	229.7	236.4
BAR	198.3	198.2	200.2	212.1	206.6	213.3
REG	248.3	248.2	252.1	289.6	287.4	291.9
FPK	255.1	254.9	259.1	289.9	287.4	292.6
BUD	265.7	265.4	269.1	313.4	311.9	315.8
PAY	275.6	275.1	279.6	319.1	317.6	321.2
CAR	291.9	291.5	296.0	314.4	312.6	317.1
PSU	251.5	251.8	255.0	304.9	304.1	307.4
BOU	203.2	205.0	207.9	255.9	251.2	259.7
BON	281.7	281.6	285.1	330.6	329.5	332.9
DRN	250.1	251.8	254.9	274.5	273.1	278.5
SGP	292.9	292.9	296.6	337.7	337.0	341.0
TAT	278.2	277.6	281.9	329.2	328.0	331.0
GWN	301.4	301.2	305.0	353.7	352.9	357.0
BER	304.6	305.0	308.1	363.2	363.0	365.5
KWA	n/a	n/a	n/a	410.6	410.4	416.4
ILO	405.4	405.8	412.1	413.8	413.8	420.4
NAU	n/a	n/a	n/a	411.3	411.2	417.1
MAN	n/a	n/a	n/a	426.0	426.0	430.9
ALS	284.9	285.2	288.8	303.7	302.9	306.9
FLO	277.6	277.9	281.4	355.3	354.9	357.8
SYO	152.1	153.5	153.4	211.1	198.1	216.6
GVN	147.9	149.3	148.9	200.0	190.0	204.3
SPO	69.2	71.1	72.8	77.5	76.9	85.9

Table 4: Impact of a change in longwave radiation scheme on the surface downward longwave radiation.

Calculations are done for the 1464 one-hour intervals of the period April-May 1999. M'91 is the longwave radiation scheme (Morcrette, 1991) operational till December 1997, also used for ERA-15; G'00 is the revised M'91 (Gregory et al., 2000) used between December 1997 and June 2000; RRTM is the Rapid Radiation Transfer Model of Mlawer et al. (1997), operational since. Clear-sky situations are chosen from a model-simulated zero total cloudiness. All cloudy radiative computations assume no inhomogeneity effect. All SDLWs in Wm^{-2}.

Station	Overcast			Total		
	SS'92	SR'97	LL'00	SS'92	SR'97	LL'00
NYA	303.5	303.6	304.4	236.4	236.8	238.4
BAR	256.5	257.8	262.5	213.3	213.6	215.0
REG	332.8	332.8	333.3	291.9	291.9	292.3
FPK	314.5	314.6	315.9	292.6	292.7	293.2
BUD	328.1	328.1	328.7	315.8	315.8	316.2
PAY	363.6	363.6	364.1	321.2	321.2	321.7
CAR	354.8	354.8	355.1	317.1	317.1	317.5
PSU	345.8	345.8	345.9	307.4	307.4	307.7
BOU	293.3	293.3	293.6	259.7	259.8	260.5
BON	353.8	353.9	354.3	332.9	333.0	333.3
DRN	n/a	n/a	n/a	278.5	278.6	278.8
SGP	402.0	401.9	401.8	341.0	341.0	341.2
TAT	335.9	335.8	335.9	331.0	331.0	331.2
GWN	n/a	n/a	n/a	357.0	357.0	357.2
BER	386.7	386.7	386.9	365.5	365.5	365.9
KWA	418.5	418.5	418.6	416.4	416.3	416.4
ILO	445.4	445.4	445.5	420.4	420.4	420.6
NAU	423.7	423.7	424.1	417.1	417.1	417.2
MAN	429.5	429.5	429.6	430.9	430.9	431.1
ALS	n/a	n/a	n/a	306.9	306.9	307.2
FLO	369.1	369.1	369.3	357.8	357.8	358.0
SYO	232.6	235.2	237.0	216.6	216.8	218.9
GVN	n/a	n/a	n/a	204.3	204.5	205.7
SPO	76.8	76.8	76.8	85.9	85.9	85.9

Table 5: Sensitivity of the surface downward longwave radiation to the representation of the liquid water cloud optical properties.

Calculations are done for the 1464 one-hour intervals of the period April-May 1999, with RRTM as LW radiation scheme. Results are presented for all-sky or overcast (TCC > 0.99) conditions. All cloudy radiative computations assume no inhomogeneity effect. All ice clouds have cloud optical properties from Ebert and Curry (1992). For liquid water cloud optical properties, SS"92 refer to Smith and Shi (1992), SR'97 to Savijarvi and Raisanen (1997), and LL'00 to Lindner and Li (2000). All SDLWs in Wm^{-2}.

Station	Overcast				Total			
	SS'92	EC'92	FL'93	Fu'98	SS'92	EC'92	FL'93	Fu'98
NYA	303.7	303.5	303.5	303.5	240.6	236.4	237.1	236.3
BAR	263.4	256.5	257.7	256.2	217.5	213.3	213.9	213.1
REG	333.9	332.8	333.0	332.8	293.0	291.9	292.0	291.8
FPK	317.0	314.5	314.9	314.4	293.9	292.6	292.8	292.6
BUD	330.5	328.1	328.6	328.0	316.4	315.8	315.9	315.7
PAY	364.9	363.6	363.9	363.6	321.9	321.2	321.3	321.2
CAR	354.8	354.8	354.8	354.8	318.1	317.1	317.2	317.0
PSU	345.9	345.8	345.8	345.8	308.0	307.4	307.5	307.4
BOU	293.5	293.3	293.3	293.3	262.2	259.7	260.2	259.6
BON	355.4	353.8	354.1	353.7	333.5	332.9	333.1	332.9
DRN	n/a	n/a	n/a	n/a	279.9	278.5	278.8	278.5
SGP	402.0	402.0	402.0	402.0	341.5	341.0	341.1	341.0
TAT	335.7	335.9	336.3	335.7	331.7	331.0	331.1	330.9
GWN	n/a	n/a	n/a	n/a	357.5	357.0	357.1	357.0
BER	386.9	386.7	386.7	386.7	365.7	365.5	365.6	365.5
KWA	419.0	418.5	418.7	418.5	416.7	416.4	416.5	416.4
ILO	445.5	445.4	445.5	445.4	420.6	420.4	420.4	420.4
NAU	424.2	423.7	423.9	423.8	417.2	417.1	417.1	417.1
MAN	429.9	429.5	429.7	429.5	431.2	430.9	431.1	431.0
ALS	n/a	n/a	n/a	n/a	307.8	306.9	307.0	306.9
FLO	370.1	369.1	369.3	369.1	358.0	357.8	357.9	357.8
SYO	243.3	237.0	238.3	236.7	222.1	216.6	217.7	216.4
GVN	n/a	n/a	n/a	n/a	208.9	204.3	205.1	204.1
SPO	78.3	76.8	77.2	76.9	95.4	85.9	87.7	86.2

Table 6: Sensitivity of the surface downward longwave radiation to the representation of the ice water cloud optical properties.

Calculations are done for the 1464 one-hour intervals of the period April-May 1999, with RRTM as LW radiation scheme. Results are presented for all-sky or overcast (TCC > 0.99) conditions. All cloudy radiative computations assume no inhomogeneity effect. All liquid water clouds have cloud optical properties from Smith and Shi (1992). For ice water cloud optical properties, SS"92 refer to Smith and Shi (1992), EC'92 to Ebert and Curry (1992), FL'93 to Fu and Liou (1993), and Fu'98 to Fu et al. (1998). All SDLWs in Wm^{-2}.

Station	Overcast			Total		
	f(P)	fixed	M'94	f(P)	fixed	M'94
NYA	303.5	303.5	303.6	236.4	236.4	236.5
BAR	256.4	256.5	256.8	213.3	213.3	213.4
REG	332.8	332.8	332.9	291.8	291.9	291.9
FPK	314.4	314.5	314.5	292.6	292.6	292.6
BUD	328.0	328.1	328.1	315.7	315.8	315.8
PAY	363.6	363.6	363.7	321.2	321.2	321.2
CAR	354.8	354.8	354.8	317.0	317.1	317.1
PSU	345.8	345.8	345.8	307.4	307.4	307.4
BOU	293.3	293.3	293.3	259.6	259.7	259.7
BON	353.7	353.8	353.8	332.9	332.9	333.0
DRN	n/a	n/a	n/a	278.5	278.5	278.5
SGP	402.0	402.0	402.0	341.0	341.0	341.0
TAT	335.9	335.9	335.9	331.0	331.0	331.0
GWN	n/a	n/a	n/a	357.0	357.0	357.0
BER	386.7	386.7	386.7	365.5	365.5	365.5
KWA	418.5	418.5	418.5	416.3	416.4	416.4
ILO	445.4	445.4	445.4	420.4	420.4	420.4
NAU	423.7	423.7	423.8	417.1	417.1	417.1
MAN	429.5	429.5	429.5	430.9	430.9	431.0
ALS	n/a	n/a	n/a	306.9	306.9	306.9
FLO	369.1	369.1	369.1	357.8	357.8	357.8
SYO	236.9	237.0	237.0	216.6	216.6	216.7
GVN	n/a	n/a	n/a	204.2	204.3	204.3
SPO	76.8	76.8	76.8	85.9	85.9	85.9

Table 7: Sensitivity of the surface downward longwave radiation to the representation of the effective radius in liquid water clouds.

Calculations are done for the 1464 one-hour intervals of the period April-May 1999, with RRTM as LW radiation scheme. Results are presented for all-sky or overcast (TCC > 0.99) conditions. All cloudy radiative computations assume no inhomogeneity effect. Optical properties are from Ebert and Curry (1992) for ice clouds, and from Smith and Shi (1992) for liquid water clouds. For the effective radius in liquid water clouds, f(P) is a function of pressure, fixed refers to 10 μm over land and 13 μm over the ocean, and M'94 is the parametrization by Martin et al. (1994). All SDLWs in Wm^{-2}.

Station	Overcast				Total			
	40	40-130	30-60	S'01	40	40-130	30-60	S'01
NYA	303.6	303.4	303.5	303.7	238.1	233.8	236.4	238.3
BAR	259.5	251.5	256.5	259.1	214.9	210.9	213.3	215.5
REG	333.3	332.2	332.8	333.6	292.3	291.3	291.9	292.9
FPK	315.6	312.3	314.5	315.8	293.1	291.9	292.6	293.6
BUD	329.1	326.5	328.1	330.3	316.0	315.4	315.8	316.3
PAY	364.3	362.5	363.6	364.4	321.5	320.8	321.2	321.8
CAR	354.8	354.8	354.8	354.8	317.5	316.5	317.1	318.0
PSU	345.8	345.8	345.8	345.9	307.6	307.2	307.4	308.0
BOU	293.4	293.1	293.3	293.3	260.8	257.9	259.7	261.3
BON	354.5	353.1	353.8	355.2	333.2	332.6	332.9	333.5
DRN	n/a	n/a	n/a	n/a	279.1	277.7	278.5	279.7
SGP	402.0	402.0	402.0	402.0	341.2	340.8	341.0	341.5
TAT	336.8	334.0	335.9	337.1	331.2	330.7	331.0	331.8
GWN	n/a	n/a	n/a	n/a	357.2	356.7	357.0	357.5
BER	386.7	386.7	386.7	387.1	365.6	365.4	365.5	365.7
KWA	418.6	418.4	418.5	419.3	416.4	416.2	416.4	416.8
ILO	445.4	445.4	445.4	445.8	420.4	420.3	420.4	420.6
NAU	423.8	423.5	423.7	424.4	417.1	417.0	417.1	417.4
MAN	429.6	429.4	429.5	430.2	431.0	430.9	430.9	431.3
ALS	n/a	n/a	n/a	n/a	307.2	306.5	306.9	307.7
FLO	369.4	368.9	369.1	370.6	357.9	357.8	357.8	358.0
SYO	239.6	231.6	237.0	242.6	219.0	212.4	216.6	220.7
GVN	n/a	n/a	n/a	n/a	206.2	200.9	204.3	206.9
SPO	77.1	76.8	76.8	81.3	88.4	85.2	85.9	100.8

Table 8: Sensitivity of the surface downward longwave radiation to the representation of the effective particle size in ice water clouds.

Calculations are done for the 1464 one-hour intervals of the period April-May 1999, with RRTM as LW radiation scheme. Results are presented for all-sky or overcast (TCC > 0.99) conditions. All cloudy radiative computations assume no inhomogeneity effect. Optical properties are from Ebert and Curry (1992) for ice clouds, and from Smith and Shi (1992) for liquid water clouds. For De, the effective particle size in ice water clouds, 40 refers to a fixed De of 40 μm, 40-130 to the original diagnostic formulation f(T) of Ou and Liou (1995) with De varying between 40 and 130 μm, 30-60 to the same formulation but bounded between 30 and 60 μm, and S'01 to the diagnostic formulation f(IWC, T) of Sun (2001). All SDLWs in Wm^{-2}.

Station	Overcast		Total	
	Homog	Inhom 0.7	Homog	Inhom0.7
NYA	303.5	302.2	236.4	233.7
BAR	256.5	249.0	213.3	211.0
REG	332.8	332.0	291.9	291.0
FPK	314.5	312.3	292.6	291.7
BUD	328.1	326.7	315.8	315.2
PAY	363.6	362.7	321.2	320.5
CAR	354.8	354.6	317.1	316.3
PSU	345.8	345.7	307.4	306.9
BOU	293.3	293.0	259.7	258.1
BON	353.8	352.6	332.9	332.4
DRN	n/a	n/a	278.5	277.7
SGP	402.0	402.0	341.0	340.7
TAT	335.9	334.5	331.0	330.5
GWN	n/a	n/a	357.0	356.6
BER	386.7	386.4	365.5	365.1
KWA	418.5	418.3	416.4	416.2
ILO	445.4	445.3	420.4	420.1
NAU	423.7	423.2	417.1	416.9
MAN	429.5	429.3	430.9	430.7
ALS	n/a	n/a	306.9	306.5
FLO	369.1	368.6	357.8	357.6
SYO	237.0	233.0	216.6	213.3
GVN	n/a	n/a	204.3	201.5
SPO	76.8	76.5	85.9	83.5

Table 9: Sensitivity of the surface downward longwave radiation to the representation of the inhomogeneity effects.

Calculations are done for the 1464 one-hour intervals of the period April-May 1999, with RRTM as LW radiation scheme. Results are presented for all-sky or overcast (TCC > 0.99) conditions. Homog and Inhom0.7 respectively correspond to computations using the cloud optical properties from Smith and Shi (1992) for liquid water clouds and from Ebert and Curry (1992) for ice water clouds, using either the cloud optical thickness without scaling, or the 0.7 scaling of the optical thickness after Tiedtke (1996). All SDLWs in Wm^{-2}.

Station	Aerosols					
	Clear-sky			Total		
	No	AER1	AER2	No	AER1	AER2
NYA	213.4	213.9	213.7	233.5	233.7	233.6
BAR	199.8	200.2	200.1	210.7	211.0.	210.9
REG	251.4	252.1	251.7	290.7	291.1	290.9
FPK	258.5	259.1	258.8	291.3	291.7	291.5
BUD	267.9	269.1	268.1	314.5	315.2	314.6
PAY	278.5	279.6	278.7	320.0	320.5	320.1
CAR	294.8	296.0	294.9	315.6	316.3	315.7
PSU	254.1	255.0	254.4	306.4	306.9	306.6
BOU	207.1	207.9	207.5	257.7	258.1	257.9
BON	284.3	285.1	284.6	332.0	332.4	332.1
DRN	254.3	254.9	254.6	277.3	277.7	277.5
SGP	295.9	296.6	296.2	340.3	340.7	340.4
TAT	281.5	281.9	282.0	330.3	330.5	330.5
GWN	304.3	305.0	304.6	356.2	356.6	356.4
BER	307.1	308.1	307.4	364.7	365.1	364.8
KWA	n/a	n/a	n/a	416.1	416.2	416.2
ILO	411.1	412.1	411.2	419.4	420.1	419.4
NAU	n/a	n/a	n/a	416.9	416.9	417.0
MAN	n/a	n/a	n/a	430.7	430.7	430.7
ALS	288.4	288.8	288.9	306.2	306.5	306.6
FLO	281.1	281.4	281.6	357.5	357.6	357.6
SYO	153.2	153.4	153.7	213.2	213.3	213.4
GVN	148.7	148.9	149.2	201.4	201.5	201.7
SPO	72.6	72.8	73.7	83.4	83.5	84.3

Table 10: Impact of various climatological representations of the aerosols.

Calculations are done for the 1464 one-hour intervals of the period April-May 1999 with RRTM, without (No) or with account for the radiative effects of the aerosols. AER1 is the operational configuration with geographical distributions and optical properties from Tanre et al. (1983), AER2 is an experimental climatology with geographical distributions and optical properties from Koepke et al. (1997) and Hess et al. (1998). All cloudy radiative computations assume the inhomogeneity effect of Tiedtke (1996), the water cloud optical properties from Smith and Shi (1992), and the ice cloud optical properties from Ebert and Curry (1992). All SDLWs in Wm^{-2}.

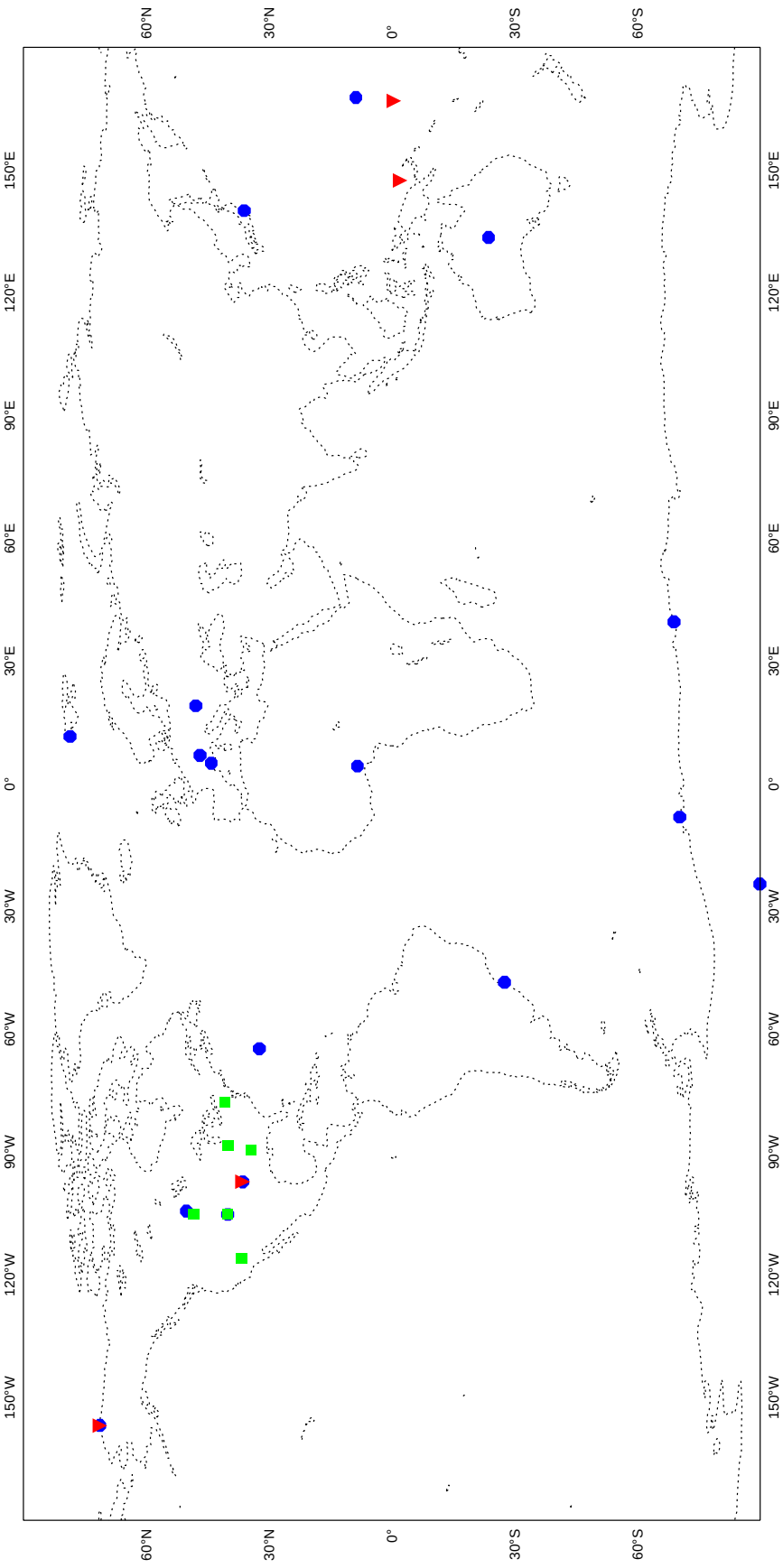

Figure 1: The geographical distribution of the surface radiation measuring stations used in this study. Circles correspond to stations belonging to the BSRN, squares to the SURFRAD, and triangles to the ARM networks.

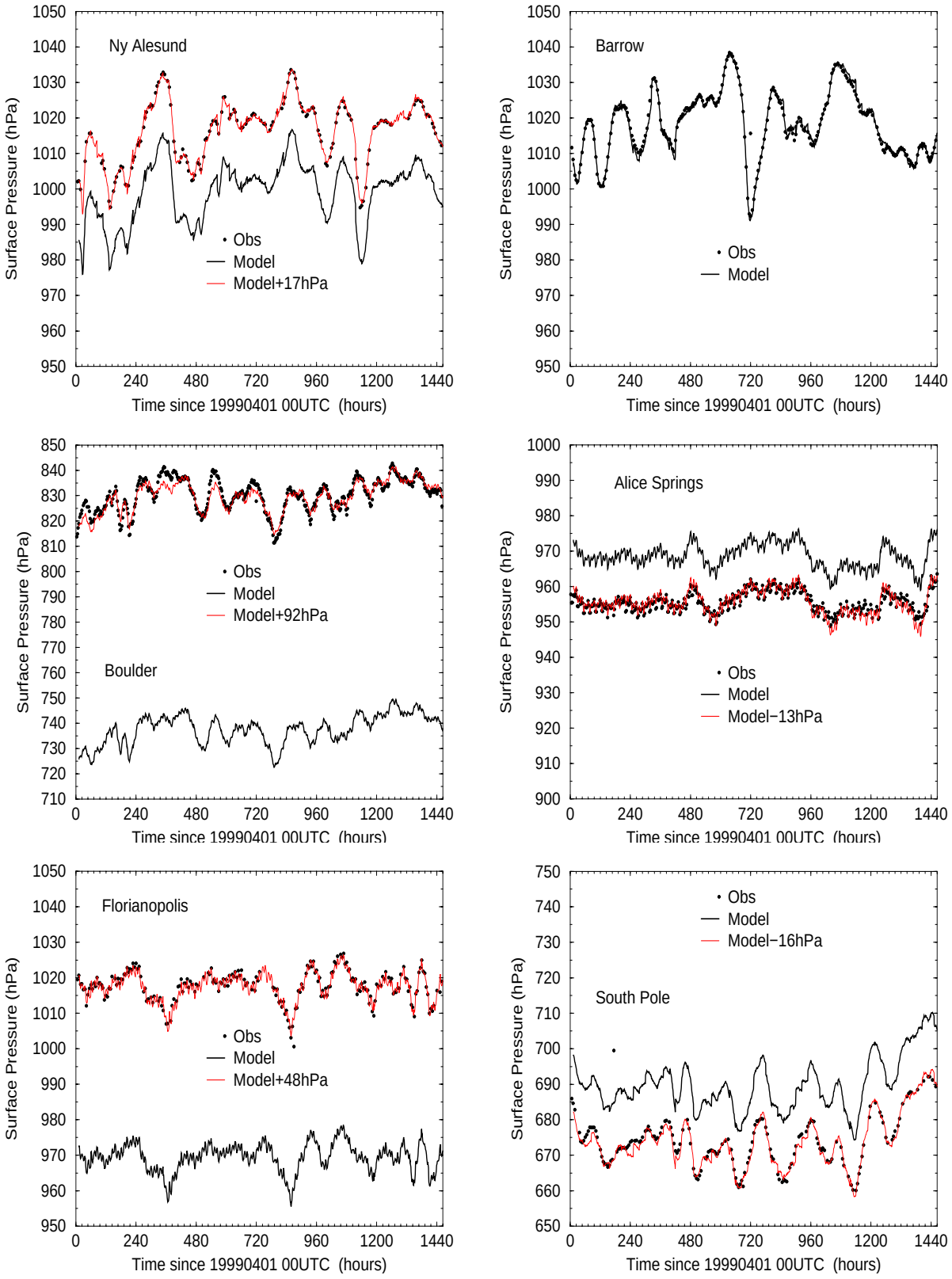

Figure 2: Surface pressure for NYA, BAR, BOU, ALS, FLO and SPO (see Table 1), observed at synoptic stations, model-produced and model-corrected (in hPa).

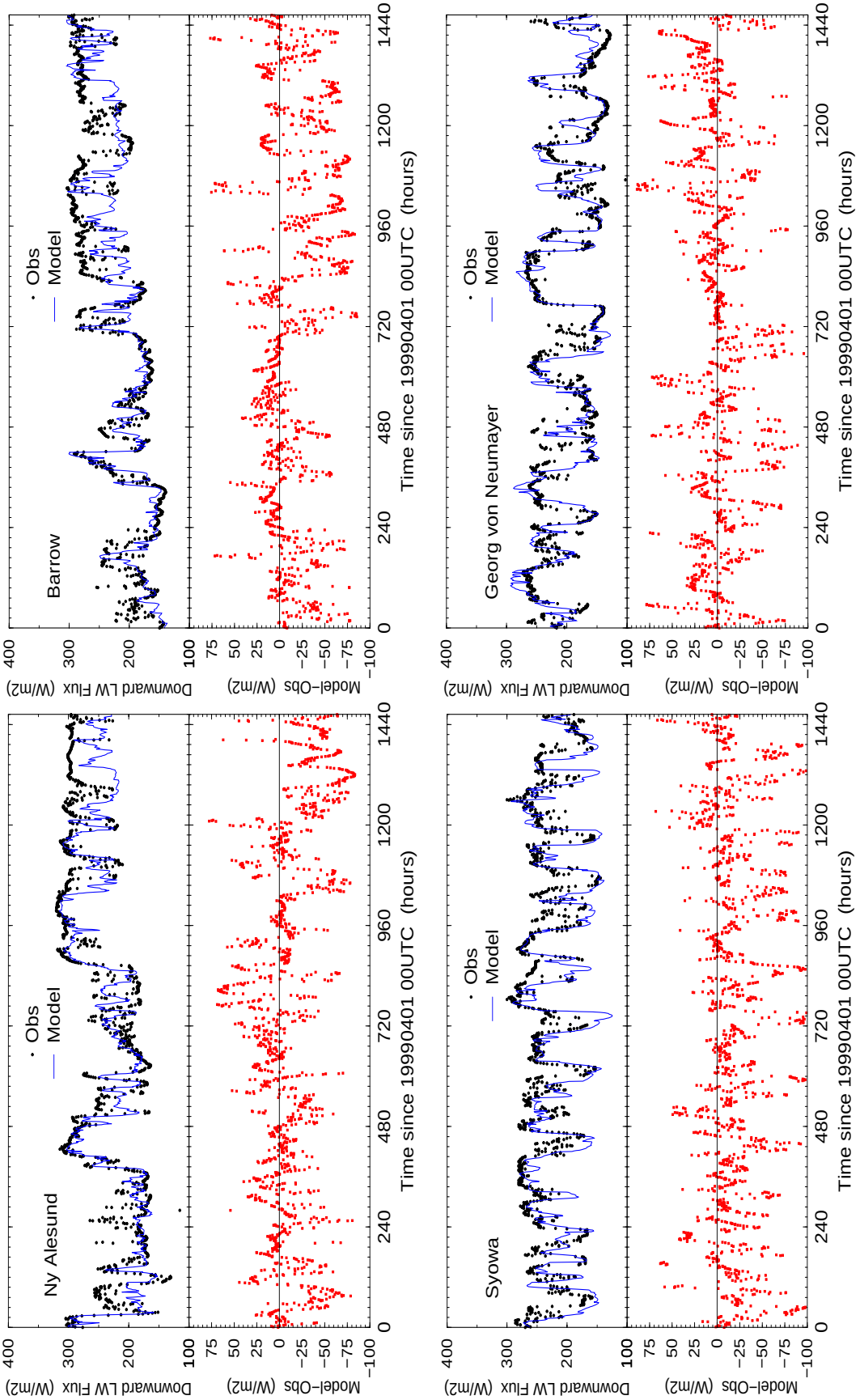

Figure 3: The surface downward longwave radiation over four high-latitude stations: Ny Alesund, Barrow, Syowa, and Georg von Neumayer. Top panels are the observed and model fluxes, bottom panels are the differences Model-Observation. All fluxes in Wm^{-2}.

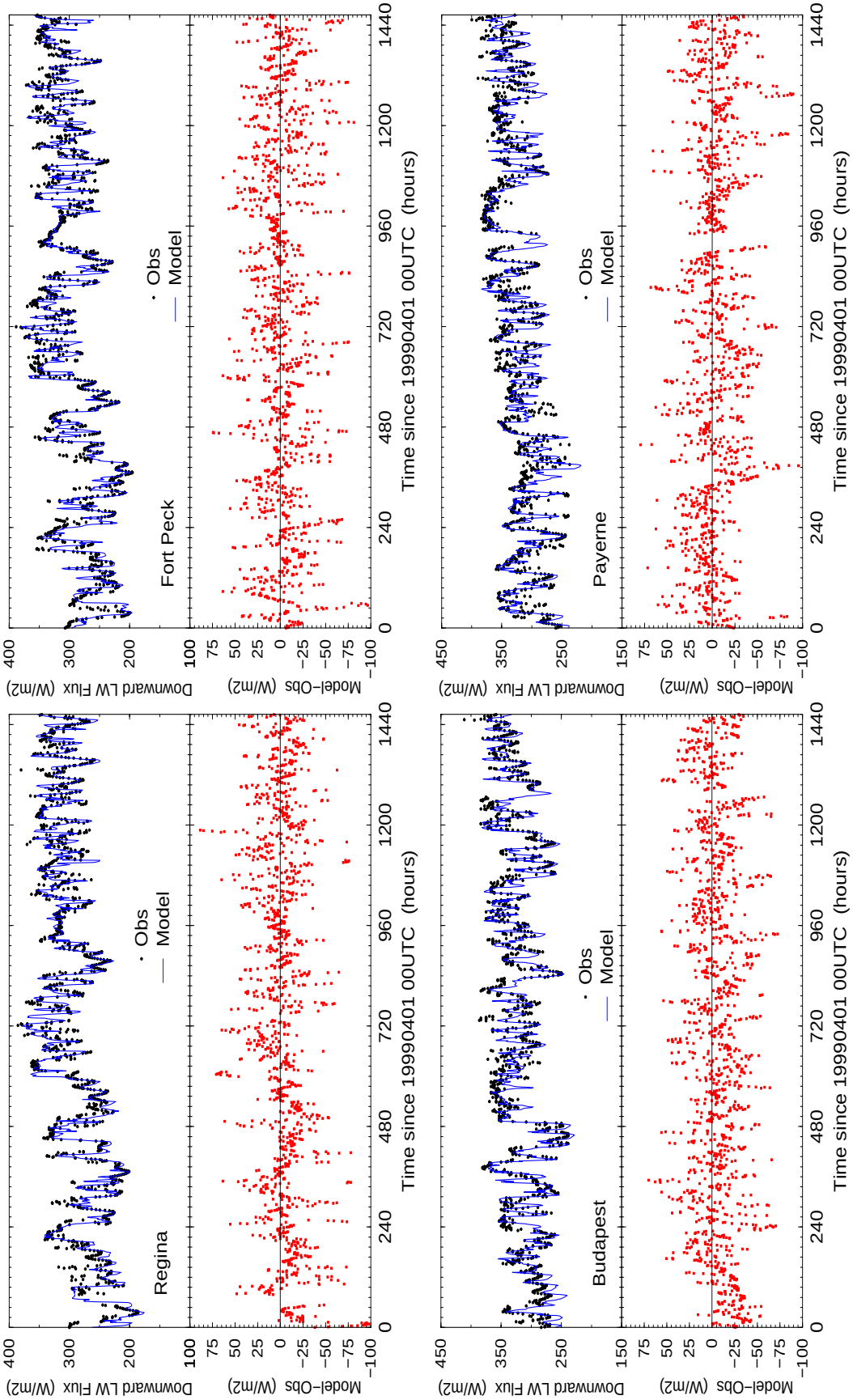

Figure 4: As in Figure 3, but for the mid-latitude stations of Regina, Fort Peck, Budapest, and Payerne.

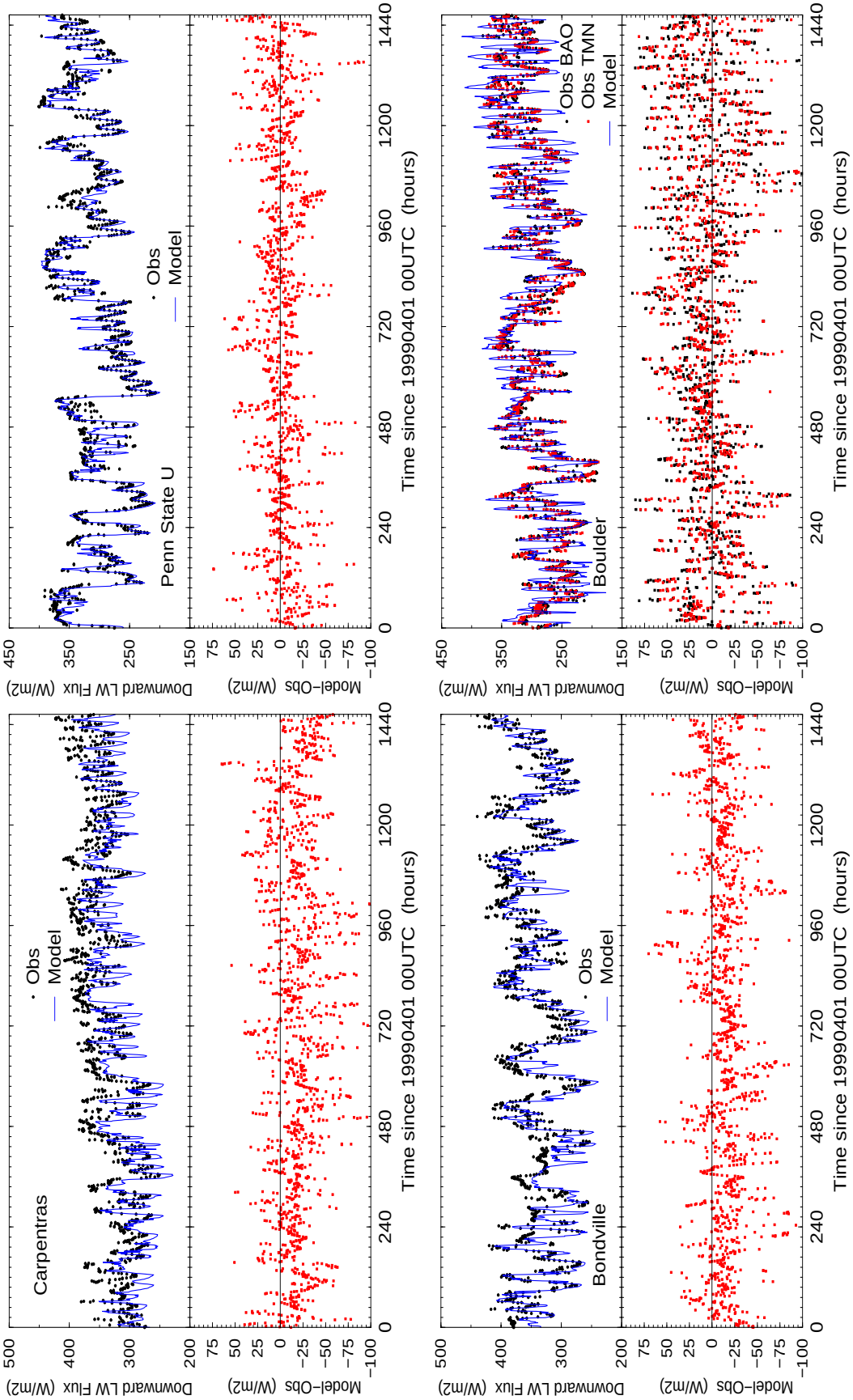

Figure 5: As in Figure 3, but for the mid-latitude stations of Carpentras, Penn State University, Bondville, and Boulder.

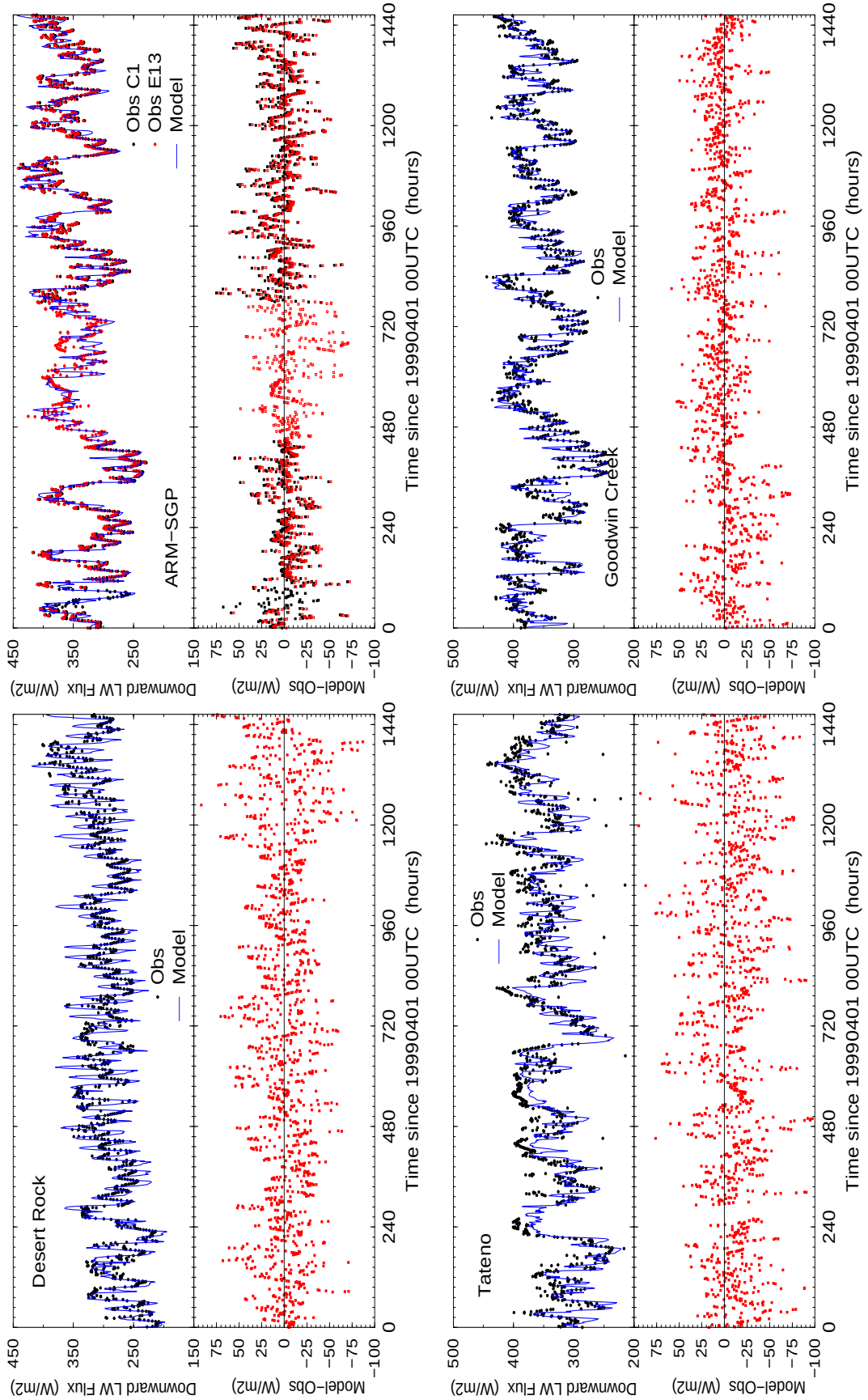

Figure 6: As in Figure 3, but for the mid-latitude stations of Desert Rock, Billings (ARM-SGP), Tateno and Goodwin Creek.

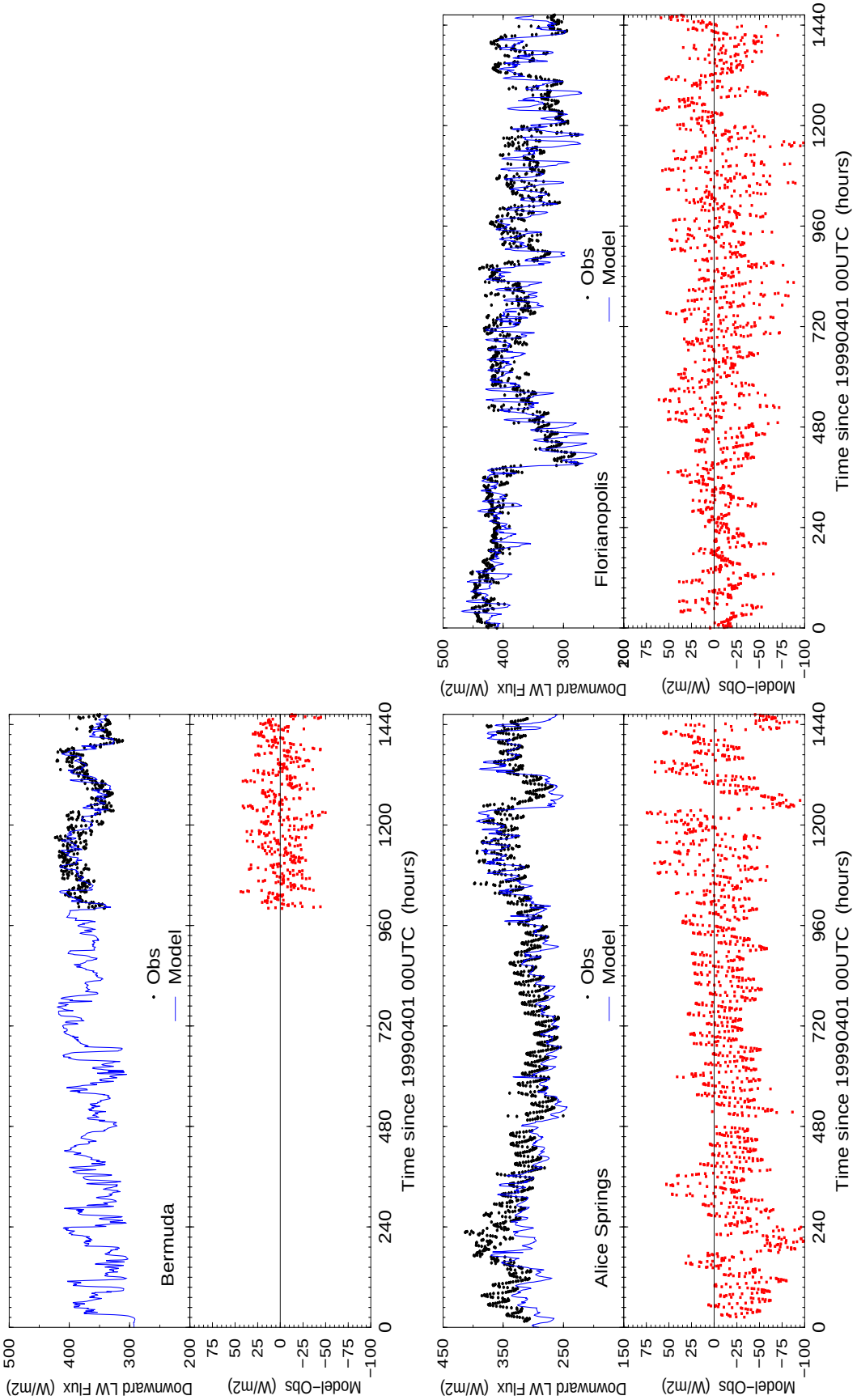

Figure 7: As in Figure 3, but for the mid-latitude stations of Bermuda, Alice Springs and Florianopolis.

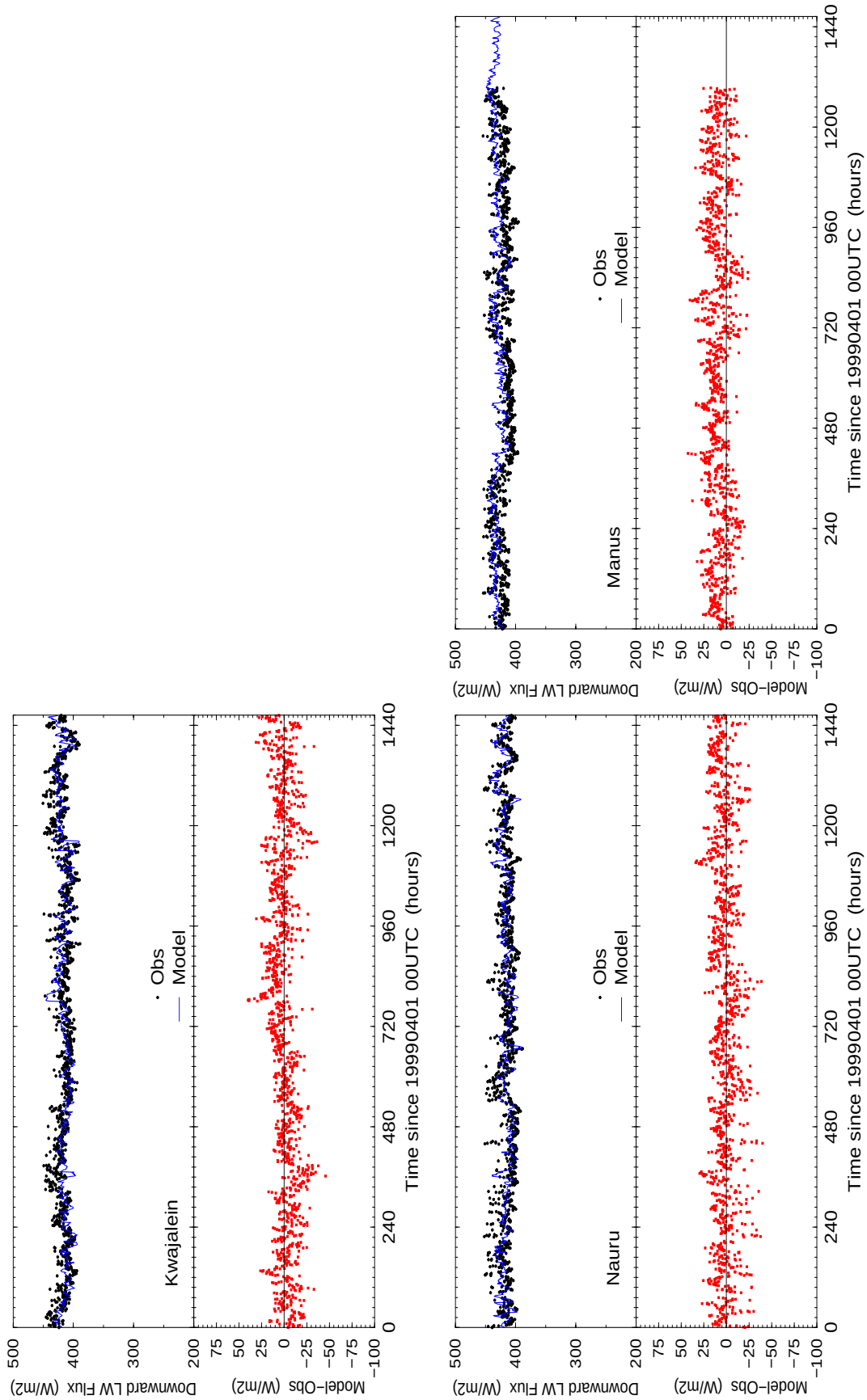

Figure 8: As in Figure 3, but for the tropical stations of Kwajalein, Nauru (ARM-TWP1) and Manus (ARM-TWP2).

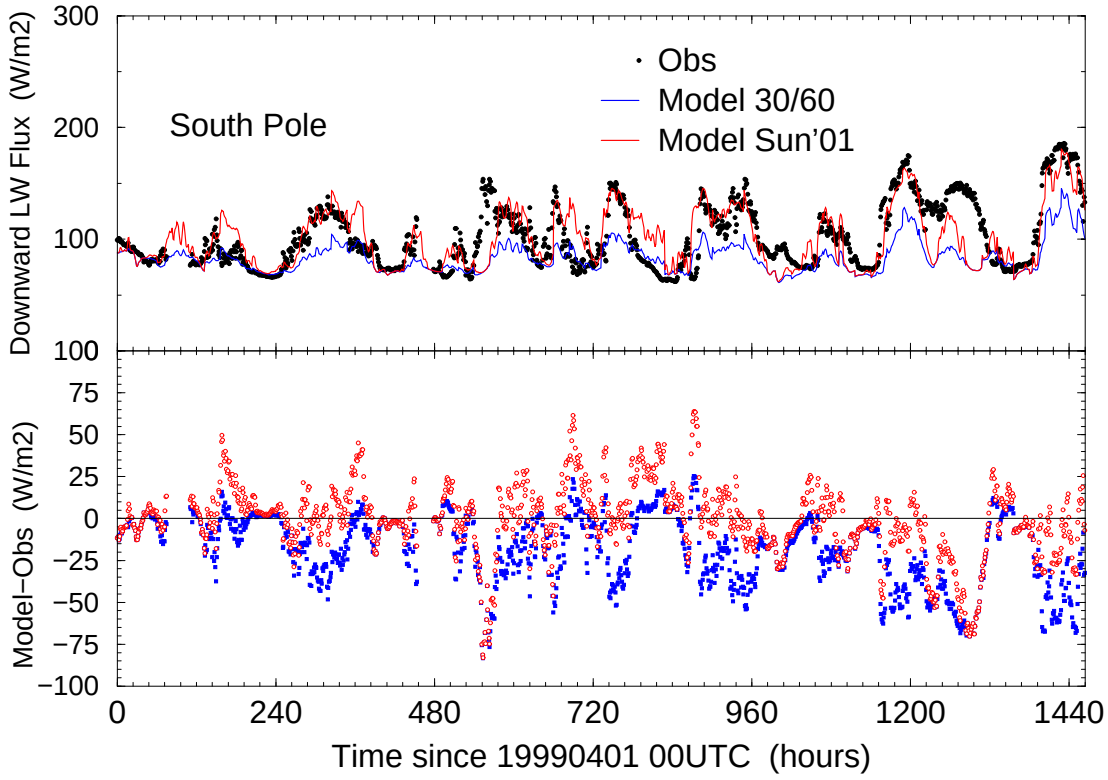

Figure 9: The surface downward longwave radiation over the South Pole. Top panel includes the observed fluxes and computed fluxes with two different sets of ice optical properties, bottom panel presents the differences Model-Observation. All fluxes in Wm^{-2}.